Retrospective Theses and Dissertations

2008

Experimental simulation of atmospheric boundary layers and extreme gust events

Emily C. Jones
Iowa State University

Follow this and additional works at: https://lib.dr.iastate.edu/rtd

Part of the Aerospace Engineering Commons

Recommended Citation

Jones, Emily C., "Experimental simulation of atmospheric boundary layers and extreme gust events" (2008). *Retrospective Theses and Dissertations*. 15334.
https://lib.dr.iastate.edu/rtd/15334

Experimental simulation of atmospheric boundary layers and extreme gust events

by

Emily C. Jones

A thesis submitted to the graduate faculty

in partial fulfillment of the requirements for the degree of

MASTER OF SCIENCE

Major: Aerospace Engineering

Program of Study Committee:
Fred L. Haan Jr., Major Professor
Partha P. Sarkar
Tom I-P. Shih

Iowa State University

Ames, Iowa

2008

المنارة للاستشارات

www.manaraa.com

DEDICATION

I would like to dedicate this thesis to Ryan and Janelle, the Aeroboys; Matt, Ben, Greg, and Tom, and my sisters of Alpha Sigma Kappa - Women in Technical Studies for their love, encouragement, understanding, and most importantly, laughter. I would also like to thank all my friends and family for their love and willingness to listen during the writing of this work.

TABLE OF CONTENTS

LIST OF TABLES

LIST OF FIGURES

CHAPTER 1.   OVERVIEW

The immense devastation caused by wind damage during extreme weather, such as tornadoes, hurricanes, and gust fronts, has highlighted the need to improve the ability of buildings, bridges, and other structures to withstand extreme winds. In determining wind loads on a building, winds are assumed to be statistically stationary. While this assumption of steady winds generates reasonable load estimates for typical weather, it is insufficient to describe the non-stationary winds encountered during storms, which are precisely the winds which may generate the greatest loads. Measurements taken at full scale show velocity increases of 15% to 50% during thunderstorms and hurricanes (1). Non-stationary winds can contain transitional flow structurs and experience rapid changes in direction that may have a significant effect upon wind loads (1). An understanding of the large gusts that can happen during extreme weather is necessary for improved protection and design of buildings, bridges, and other structures. Full scale wind velocity and pressure measurements are challenging during extreme weather, so wind tunnel simulation of gust events is a vital step in discovering the effects the gusts have, both on structures and on the atmospheric boundary layer itself. However, there has been little experimental study of large-scale gust events in the past, as typical wind tunnel flows cannot simulate non-stationary velocities.

Before atmospheric gust events could be simulated in the Iowa State University Aerodynamic - Atmospheric Boundary Layer (AABL) Wind and Gust Tunnel, the atmospheric boundary layer had to be modeled for several terrain types. Scaled open, suburban, and urban terrains were all simulated using stationary turbulence-generating obstacles. The effects of these obstacles were studied in order to simplify simulation of additional boundary layers for

future projects.

The bypass duct gusting system was used to generate various gust events within the three atmospheric boundary layers simulated. The gusting system uses damper vanes within a bypass duct that can open or close to respectively decrease or increase mean flow velocity. As this was the first use of the computerized gusting system, the types of gusts it can produce were explored to determine the appropriate settings for a range of typical gust events. After parameters for the gust events were selected, the resulting velocity data were analyzed using wavelet theory. The data analysis centered around turbulence intensity, although Reynolds stresses were also considered. This analysis demonstrated that the gust events had no measureable effect on these components of the atmospheric boundary layer.

CHAPTER 2. ATMOSPHERIC BOUNDARY LAYER SIMULATION

2.1 Introduction

The initial task in this investigation was to develop reasonable scaled simulations of the atmospheric boundary layer (ABL) for several terrain types: open, suburban, and urban. The generation of atmospheric boundary layers was performed mechanically in the Aerodynamic - Atmospheric Boundary Layer (AABL) Wind and Gust Tunnel, using stationary obstacles to introduce turbulence into the flow. Two building codes, ASCE7-05 (2) from the U.S.A. and AIJ (3) from Japan were selected as standards for the scaled boundary layers. While matching mean velocity and turbulence intensity profiles corresponding to the three terrain types were the main objectives, an investigation of the individual effects of the turbulence devices was also conducted, in order to expedite the boundary layer simulation process in the future as needs for additional atmospheric boundary layers develop.

2.2 Selected Standards

There are two sets of criteria generally used to determine whether an appropriate simulation has been achieved, a set of aerodynamic quantities and profiles of the mean velocity and turbulence intensity. Aerodynamic quantities commonly used to describe an atmospheric boundary flow include aerodynamic roughness length, Jensen number, and boundary layer depth. The aerodynamic roughness length describes how rough a particular terrain is, so it would seem an obvious choice when trying to simulate the flow over certain terrains. The aerodynamic roughness length is estimated using properties of the log-layer in the ABL (4), so it is challenging to estimate accurately in a small scale setting, as the turbulent flow does not always settle into equilibrium within the limited length of a wind tunnel. The Jensen

number, the ratio of model or building height to aerodynamic roughness length, is thus equally challenging to match. Fang (5) and Tieleman (6) found that matching the Jensen number was not sufficient to determine an ABL match between natural and experimental data, in part because it does not quantify the turbulence generated. Boundary layer depth seems to be another straightforward value to measure, but with the height limitations imposed by the size of the AABL Wind and Gust tunnel, it is not always possible to simulate the entire atmospheric boundary layer. The second set of criteria, mean wind speed and turbulence intensity profiles, were preferred standards in several studies (7; 6). Many modern ABL studies (8; 9; 7; 10) use these profiles to prove that their boundary layers are accurately simulated.

2.2.1 Target Profiles

Atmospheric boundary layers were developed for three terrains in the AABL Wind and Gust Tunnel; open terrain, suburban terrain, and urban terrain. The standards selected to define these categories were the American and Japanese building codes, ASCE7-05 and AIJ, respectively. The ASCE7-05 (2) was selected to define these profiles because as the American building code it was the standard most likely to be followed by users of this facility. The ASCE7-05 did not contain explicit definitions of turbulence intensity and it combines suburban and urban terrain, so the AIJ building code (3) was used as a supplement. The Japanese code was selected because when plotted, its profile for open terrain mean velocity was indistinguishable from that of the ASCE7-05, and it was the most readily available of those building codes commonly used as experimental ABL standards. The experimental turbulence intensity (Iu) compared to the AIJ was defined as the ratio of the velocity variance and the mean velocity.

2.2.2 Scaling

The selection of the scale at which to simulate the ABL was a compromise between building model size and ceiling interference. At a small scale, such as 1:1000, a model of a house would be too small relative to the roughness elements for building geometry to have a measureable effect, whereas a large scale like 1:5 could have wind tunnel blockage effects within the portion

of the boundary layer containing the model. Considering the size of the AABL tunnel, a scale of 1:100 was determined a reasonable compromise between these two trade-offs.

2.2.3 Pressure Gradient

In order to reduce the effects of the wind tunnel ceiling, the adjustable ceiling of the wind tunnel was shifted to produce a pressure gradient of zero, with an accuracy of 8%, across the test section. Additionally, a pressure gradient of zero more accurately reflects the atmospheric boundary layer. The ceiling configurations are listed in Table 2.1. The locations the ceiling heights were measured at correspond to the points attached to the adjustment cables, from upstream to downstream ends.

Table 2.1   Ceiling heights used to reduce wind tunnel pressure gradient, measured at adjustment cables from upstream to downstream positions

Measurement Point	Ceiling Height Chain Configuration (in)	Ceiling Height Block Configuration (in)
1	73.5	73.5
2	73	76.5
3	72	78
4	72	79
5	73	80
6	74.5	81
7	76	81.5
8	75	82
9	75	82
10	75	81
11	75.5	83
12	79.5	84.5

2.3 Turbulence Generating Devices

Triangular spires (11), walls, blocks, and rows of chain were employed in various configurations to simulate the atmospheric boundary layers. A typical wind tunnel set up, complete with model, is displayed in Figure 2.1.
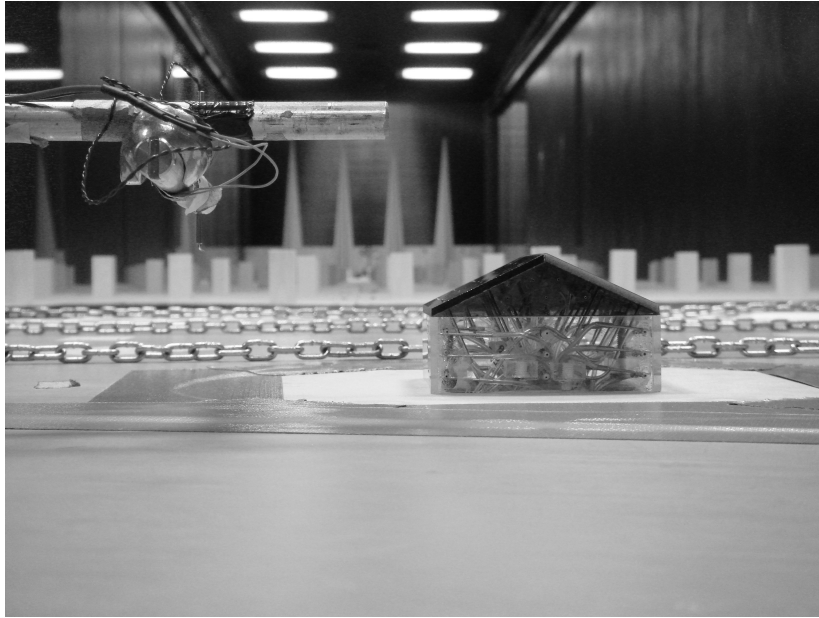
Figure 2.1 Turbulence generators in the AABL Wind and Gust Tunnel

2.3.1 Spires

Five spire sets (A-E) were built and tested, with spire height and base-to-height ratio as the main design parameters as described by Irwin (12). Only sets A-D are included in the spire study, because set E was built specifically for suburban terrain, well after the investigation of the spires was completed. Turbulence generation methods are wind tunnel specific, so some adaptations had to be made to Irwin's method, which uses the desired power law exponent, and the desired boundary layer thickness as the input parameters. Specifically, for the AABL tunnel, Irwin's method (12) allowed the design of spires to produce any power law exponent desired, as long as the assumed boundary layer thickness was four feet, rather than the calculated desired boundary layer thickness. Spire set E was successfully designed with the adapted version of Irwin's method.

Table 2.2   Spire dimensions

Spire Set	Height (in)	Base-to-height ratio	Power Law Exponent
A	61	0.11	0.16
B	46	0.11	0.18
C	55.5	0.27	0.47
D	50	0.20	0.13
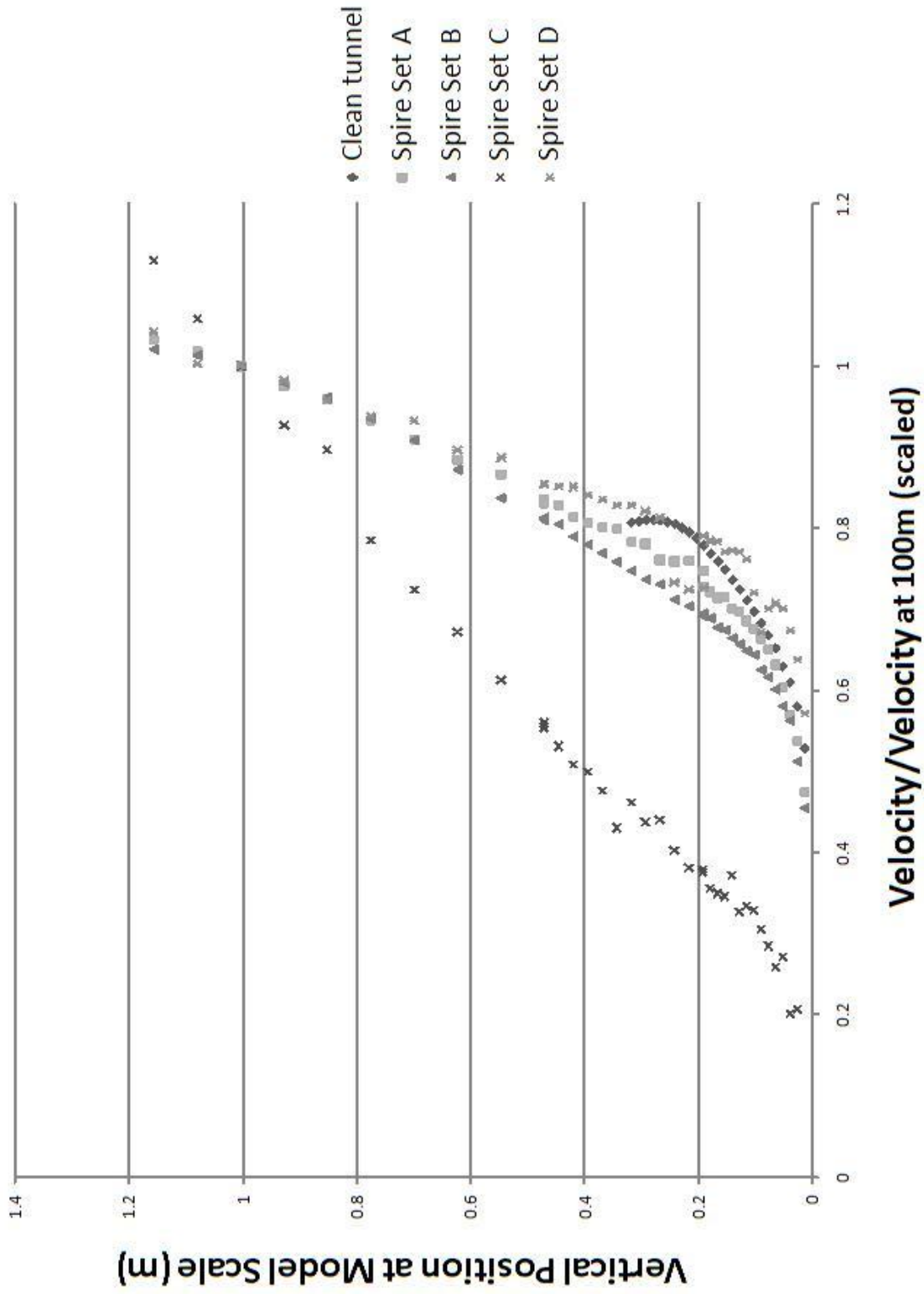
Figure 2.2 Spire effects on normalized velocity
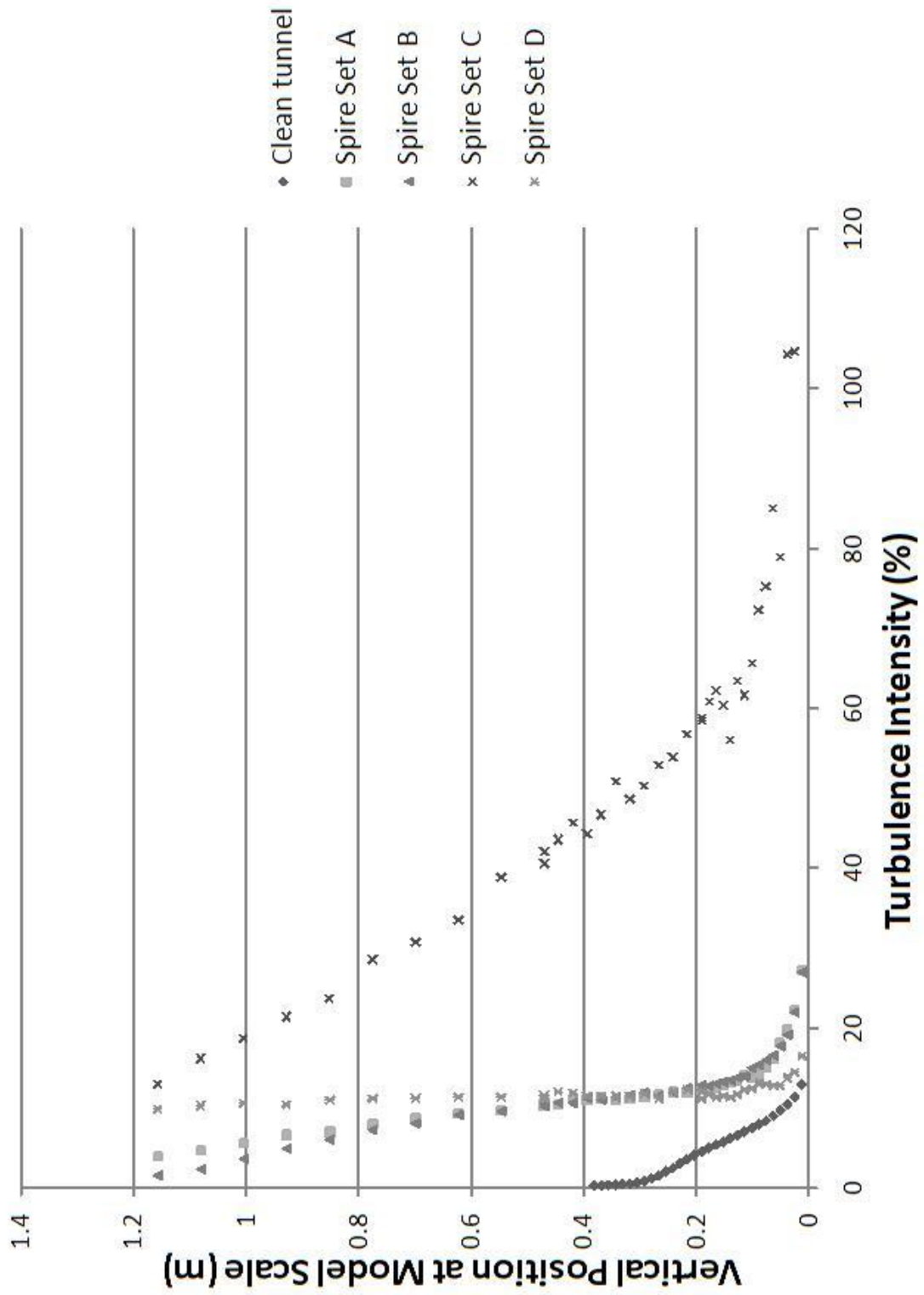
Figure 2.3   Spire effects on turbulence intensity

Most of the spires had a minimal effect on the near-ground mean velocity, as can be seen in Figure 2.2, although the largest set, C, did significantly reduce the near-ground mean velocity. The primary effects of the spires were to greatly increase the boundary layer depth and change the profile power coefficient, alpha. The variables used in the spire design were height and shape, quantified by the base-to-height ratio. Spire height, described in Table 2.2 had little impact on the mean velocity profile. Spire sets A and B had a height difference of fifteen inches, but their mean velocity profiles were very similar. As sets A and B had identical base-to-height ratios, it seemed that the shape of the spire has the most impact on the shape of the velocity profile, described by alpha. This trend was further indicated by the dissimilarity in the velocity profiles of spire sets C and D, which had a height difference of only 5.5 inches, but a significantly different base-to-height ratio. The turbulence intensity profiles in Figure 2.3 show similar trends relating turbulence intensity to spire height and shape, although less dramatically. For turbulence intensity far from the floor, the spires contributed more than any other device.

2.3.2 Floor Roughness

Two types of floor roughness were explored for the AABL facility, chains and blocks. The chains were laid in cross stream rows along a constant fetch length with two configurations; 17 rows 33 inches apart and 31 rows 16.75 inches apart. The chains, in combination with other components, successfully simulated open terrain. When it was determined that chains generated insufficient turbulence for suburban and urban terrain, regularly spaced rectangular wooden blocks were used.

2.3.2.1 Chains

Chain rows were investigated because of their simple installation, which involved wrapping one long chain with one inch links around screws located along the floor of the wind tunnel near the walls. While the chain generated some near-ground turbulence, it was a minimal effect and inadequate for generating suburban or urban turbulence intensities. When used in combination with the spires, the chains had essentially no effect on the boundary layer. Figures 2.4 and 2.5 together show that the chains had a very small effect on the ABL. Near the ground, the chains slowed the mean velocity with a corresponding increase in turbulence intensity, but their effect was limited to the bottom 0.4 meters. This slightly increased the boundary layer depth from the clean tunnel, but insufficiently for any of the desired terrains. It is useful to note that doubling the number of rows of chain had practically no effect.

2.3.2.2 Blocks

Blocks were designed using the method outlined in Gartshore (13; 14) to generate larger turbulence intensities, especially in the upper portion of the log-layer. However, Gartshore's methods (13; 14), which predict block geometry based on relationships between boundary layer characteristics and drag, seemed to be fetch length, so while the blocks used generated the predicted drag coefficient, they generated an unexpectedly low power law exponent. While Gartshore predicts the ability to generate ABL flow using only blocks (13; 14), it is important to note that his methods were tested for thinner boundary layers than those generated here. However, as the triangular spires were the primary device to effect the power law exponent, the blocks were still quite effective for increasing turbulence intensity when used in conjunction with other turbulence generators. If the need arises in future work for a flow with a significantly greater turbulence intensity, Gartshore's method would be useful as a general outline, but alternative block design methods should also be explored.

Table 2.3   Block sheet arrangements numerically arranged from upstream to downstream position. Rows 1-9 are always placed in the same location, with row 12 shifting from far downstream in Layout A to far upstream in Layout B. The letters are ordered south to north. See Figures 2.22 and 2.23.

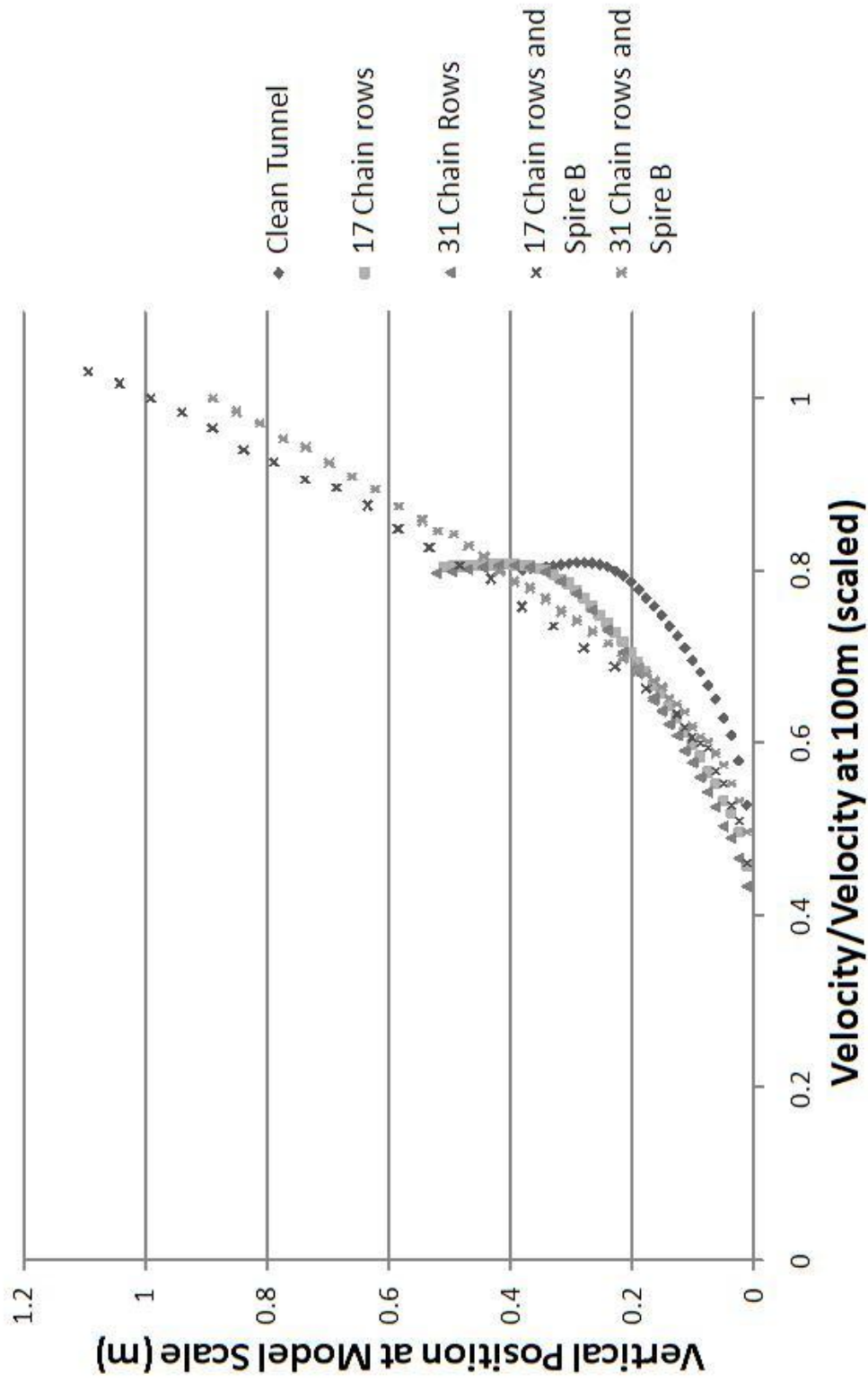| Block Layout A	Block Layout B
–	12B - 12A
9B - 9A	9B - 9A
8B - 8A	8B - 8A
7A - 7B	7B - 7A
6A - 6B	6A - 6B
5A - 5B	5A - 5B
4A - 4B	4A - 4B
3B - 3A	3A - 3B
2B - 2A	2B - 2A
1B - 1A	1B - 1A
12B - 12A	–

Figure 2.4   Chain effects on normalized velocity

15
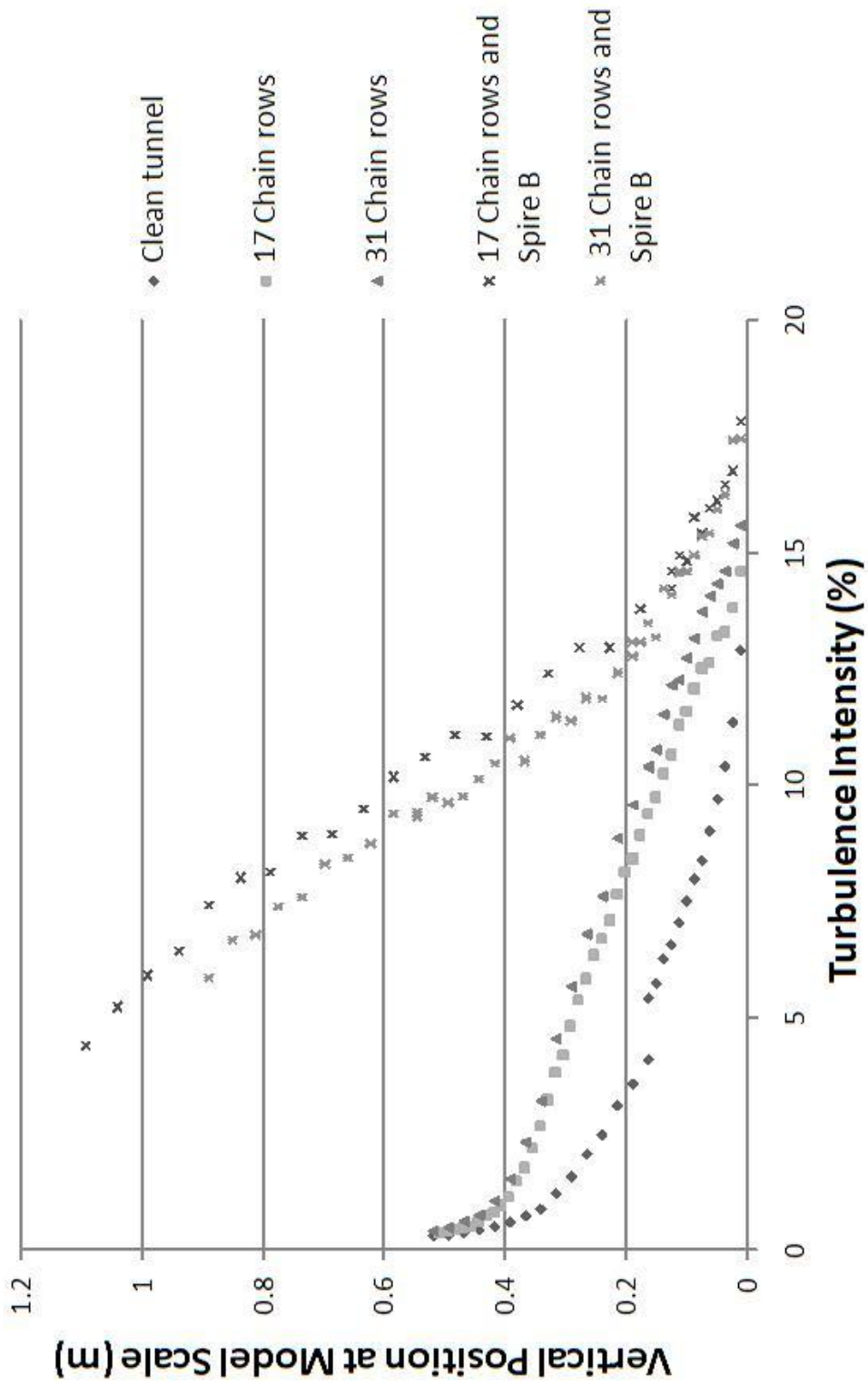
Figure 2.5 Chain effects on turbulence intensity

The block width and length is 1.5 inches, and the height is 3 inches. The blocks were spaced 15 inches apart, in staggered rows (see Figure 2.22) that were also 15 inches apart. The blocks were attached to sheets of plywood to expedite installation, with three rows of blocks were attached to each plywood sheet, and the plywood sheets were labeled in a consistent corner with a (sheet) row number and a letter. There are two sheets of blocks in each (sheet) row, which are always arranged with the labels reading (right-side-up) A-B from left to right. So in Table 2.3, if the sheets are arranged as B-A, this means that they must be rotated relative to the A-B arrangement. The row numbers in Table 2.3 correspond to the labels on the plywood sheets, not the individual block rows. Two arrangements of the blocks were used in the final profiles. Both arrangements use all nine rows, with row 12 changing from a downstream to upstream position.

Figures 2.6 and 2.7 display the mean velocity and turbulence intensity profiles for the blocks. The standard case was of 30 rows of blocks (all 10 available rows of plywood sheets) which was varied by adding chain rows alternating with the block rows (interspersed chains) and by removing the sheets most upstream and downstream, labeled as 27 Block Rows with the corresponding removal in Figures 2.6 and 2.7. The blocks generated a boundary layer about 0.6 m thick, with larger turbulence intensity than the chains. The addition of chain rows slightly increased the turbulence intensity, although it had a negligible effect on the mean velocity. Removing block rows reduced the turbulence intensity, with a larger decrease within 0.2 m of the ground. The blocks were most useful for generating turbulence intensity, rather than changing the power law exponent of the mean velocity profile.
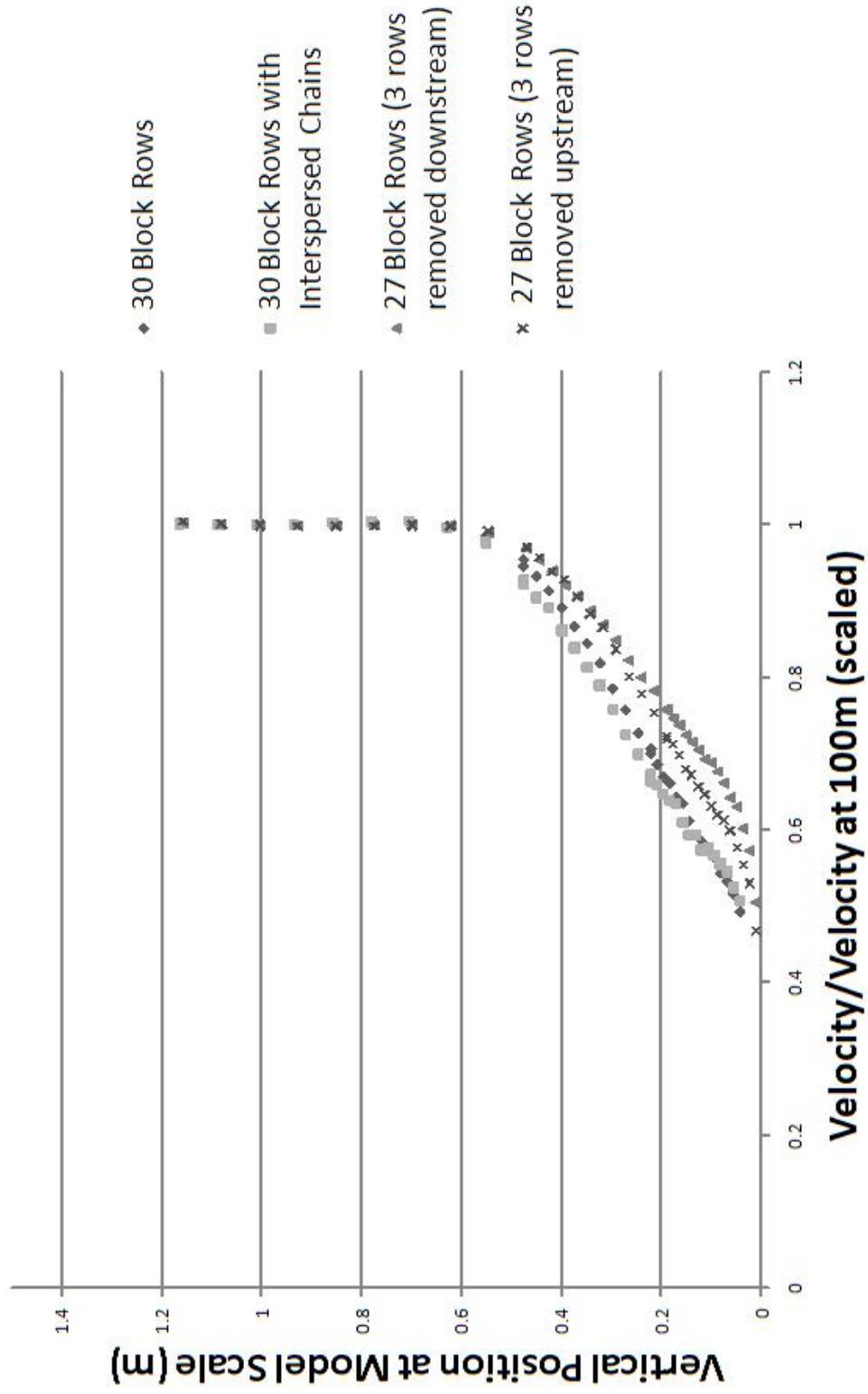
Figure 2.6　Block effects on normalized velocity
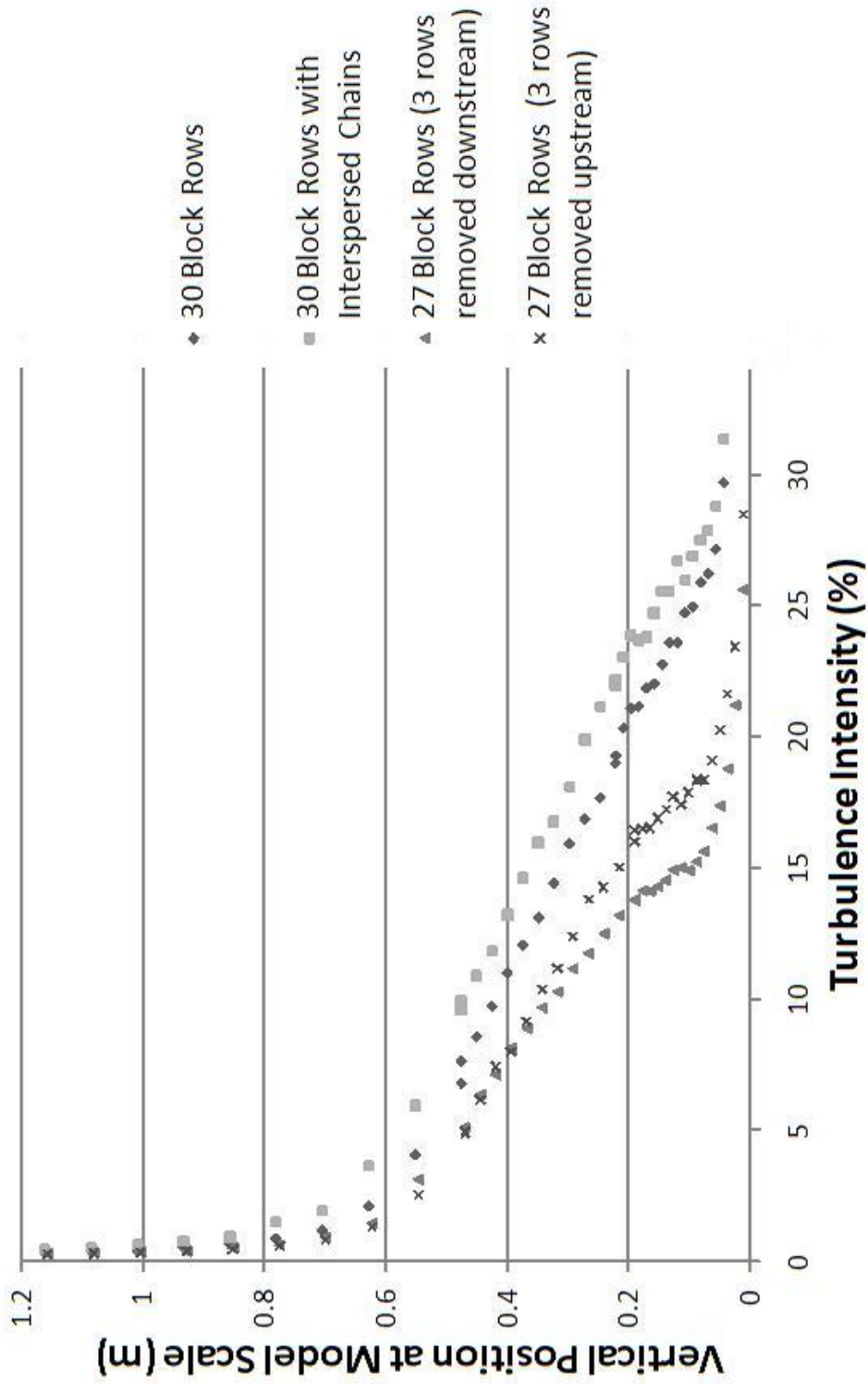
Figure 2.7   Block effects on turbulence intensity

2.3.3   Walls

While walls are generally used in any physical boundary layer simulation, there was no previous work found that investigated the physics behind the effect of the wall. It was observed that adding the wall to the wind tunnel turbulence configuration increased the turbulence intensity.
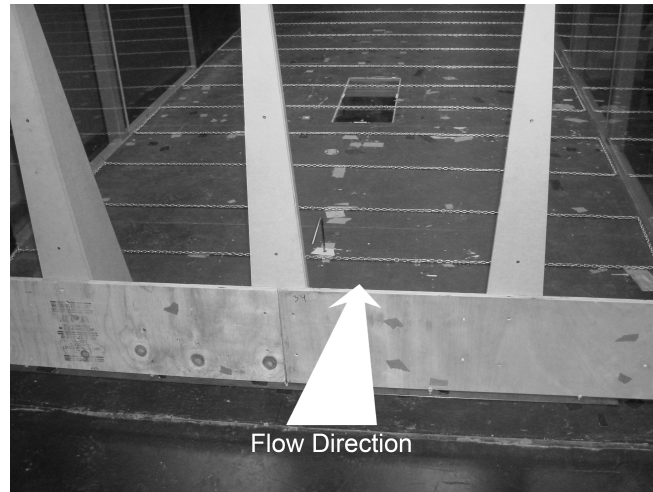
Figure 2.8   Standard wall position

There were two parameters investigated for the walls, the wall height and wall position. Wall heights of 12 in and 5 in were tested. In one case the wall was at the upstream edge of the spires as in Figure 2.8 and in the other case the wall was 24 in downstream of the spires. The distance downstream was measured from upstream edge of the spire, and was selected as a multiple of the tall wall height. In general the walls increased the turbulence intensity throughout the entire ABL, while insignificantly changing the velocity profile. The 12 in wall increased turbulence intensity by approximately twice as much as the 5 in wall, displayed in Figure 2.10. Positioning the walls downstream of the spires decreased the turbulence intensity by around one percent. As the walls were introduced to the ABL turbulence generators in order to increase turbulence intensity, the 12 wall positioned at the spires was selected for use in all three ABL configurations.

2.4   Other Equipment

All measurements for the development of the atmospheric boundary layers were taken in the Iowa State University AABL Wind and Gust Tunnel, using a hotwire probe and a TFI Cobra probe. Both probes were suspended on a traverse which could move the probes vertically. The hotwire was used in conjunction with an AA Labs anemometer and periodically calibrated to account for ambient pressure and temperature changes. Thirty data ensembles were taken for each measurement height, with a sampling time of two seconds and a sampling rate of 8000 Hz. The hotwire was used with a Labview program that saved the mean velocity and variance at each height, as well as the power spectral density function. The hotwire tests were run with a mean wind tunnel speed of 9 m/s, corresponding to a setting of 9 Hz. Faster speeds caused the probe to shake. The Cobra probe uses differences in pressure between several holes (oriented in several directions) and static pressure to acquire three components of velocity, which the hotwire cannot do. The streamwise, cross-stream, and vertical velocity components as measured by the Cobra probe, are referred to as $\mathbf{U}$, $\mathbf{V}$, and $\mathbf{W}$ respectively. For the profiles, the Cobra probe was run at 2500 Hz, with a mean wind tunnel speed of 15 m/s (setting of 15 Hz) and output four measurements for both the velocity and turbulence intensity; the $\mathbf{U}$, $\mathbf{V}$, and $\mathbf{W}$ components as well as the total.
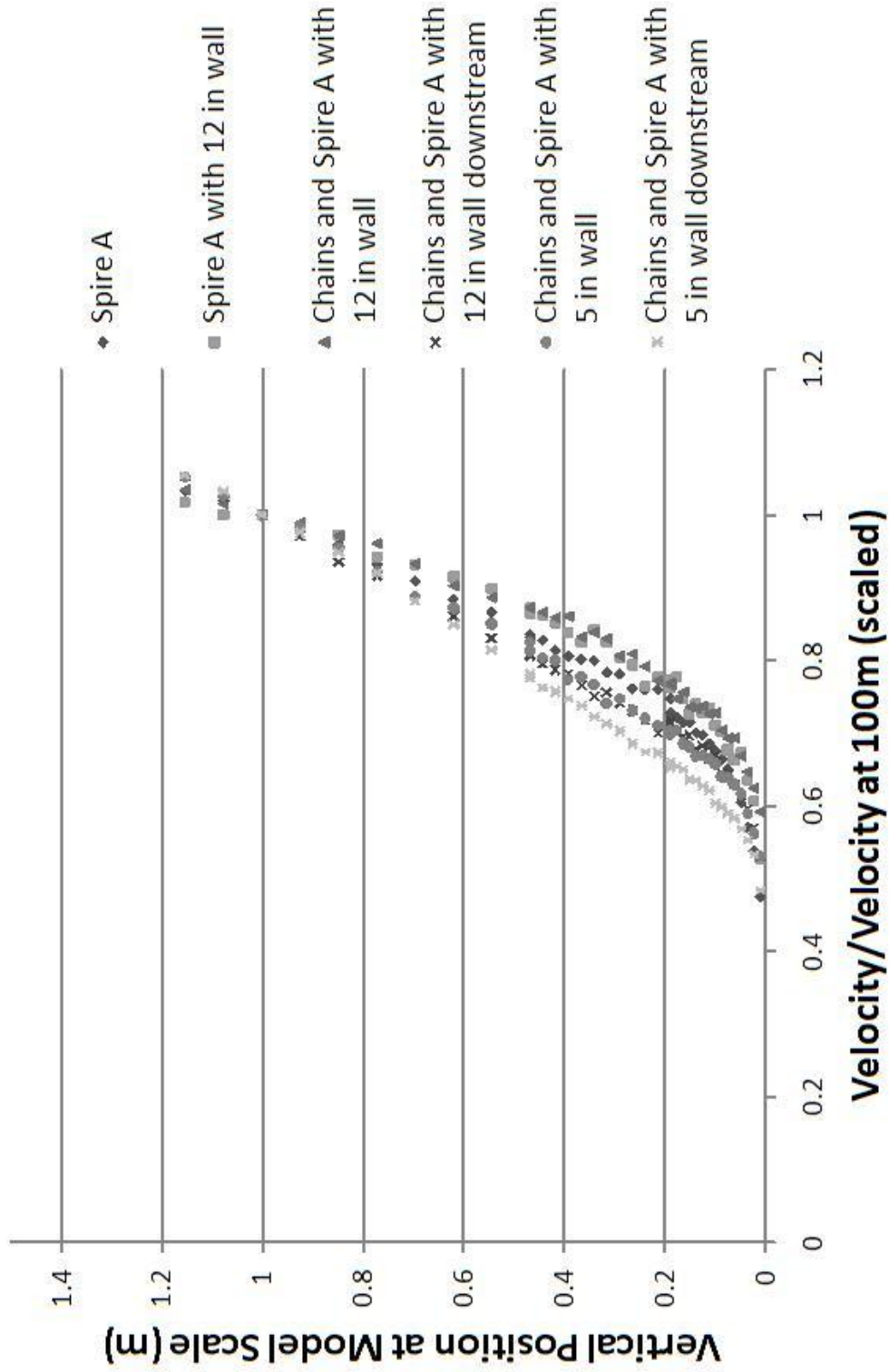
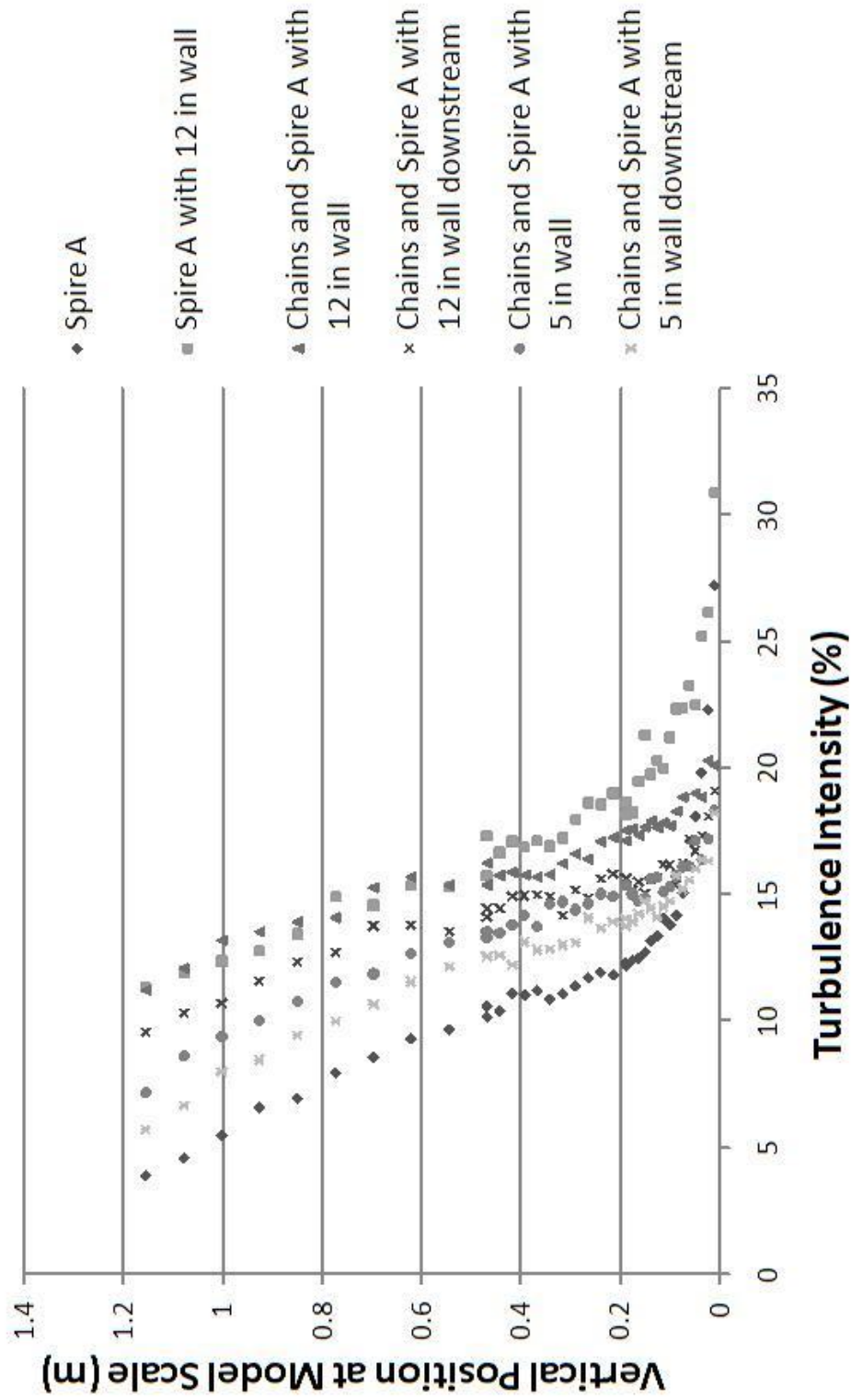Figure 2.9   Wall height effects on velocity

Figure 2.10   Wall height effects on turbulence intensity

2.5   Final Atmospheric Boundary Layers

Figures 2.11 through 2.19 display the finalized mean velocity, turbulence intensity, and spectra for open, suburban, and urban terrain at a 1:100 scale. The experimental spectra were calculated from Cobra data measured at 6 cm in the **U** direction, while the calculated spectra were generated from Tieleman's models for universal spectra (15). The measurements that were taken with the hotwire were taken with a mean wind tunnel speed of 9 m/s and a sampling speed of 8000 Hz, while those from the Cobra probe were taken at a wind tunnel speed of 15 m/s and a sampling speed of 2500 Hz. Both data sets contain measurements over 60 second intervals. The non-zero mean of the **V** component from the Cobra data indicates that the Cobra probe was not perfectly aligned with the streamwise direction. For the open and suburban terrains, Figures 2.11 through 2.15 show an excellent agreement between the two measurements, indicating independence from the mean wind tunnel speed. The urban terrain showed some dependence on wind tunnel speed, particularly in the turbulence intensity in Figure 2.18. Amelioration of this dependence has yet to be investigated, but a taller wall is likely to increase the turbulence intensity to the desired levels at the higher mean wind tunnel speeds. Table 2.4 lists some characteristic quantities of the atmospheric boundary layers. The suburban tunnel configuration, which contains all the generators described above, is displayed in Figure 2.20. The components used for each terrain are described in Tables 2.6 and 2.5, and representative (but not to scale) diagrams are displayed in Figures 2.21 through 2.23. The specific arrangement of the sheets of blocks is in Table 2.3 and the ceiling configurations are listed in Table 2.1. All wind tunnel configurations assume that measurements will be taken near the center of the wind tunnel turntable.
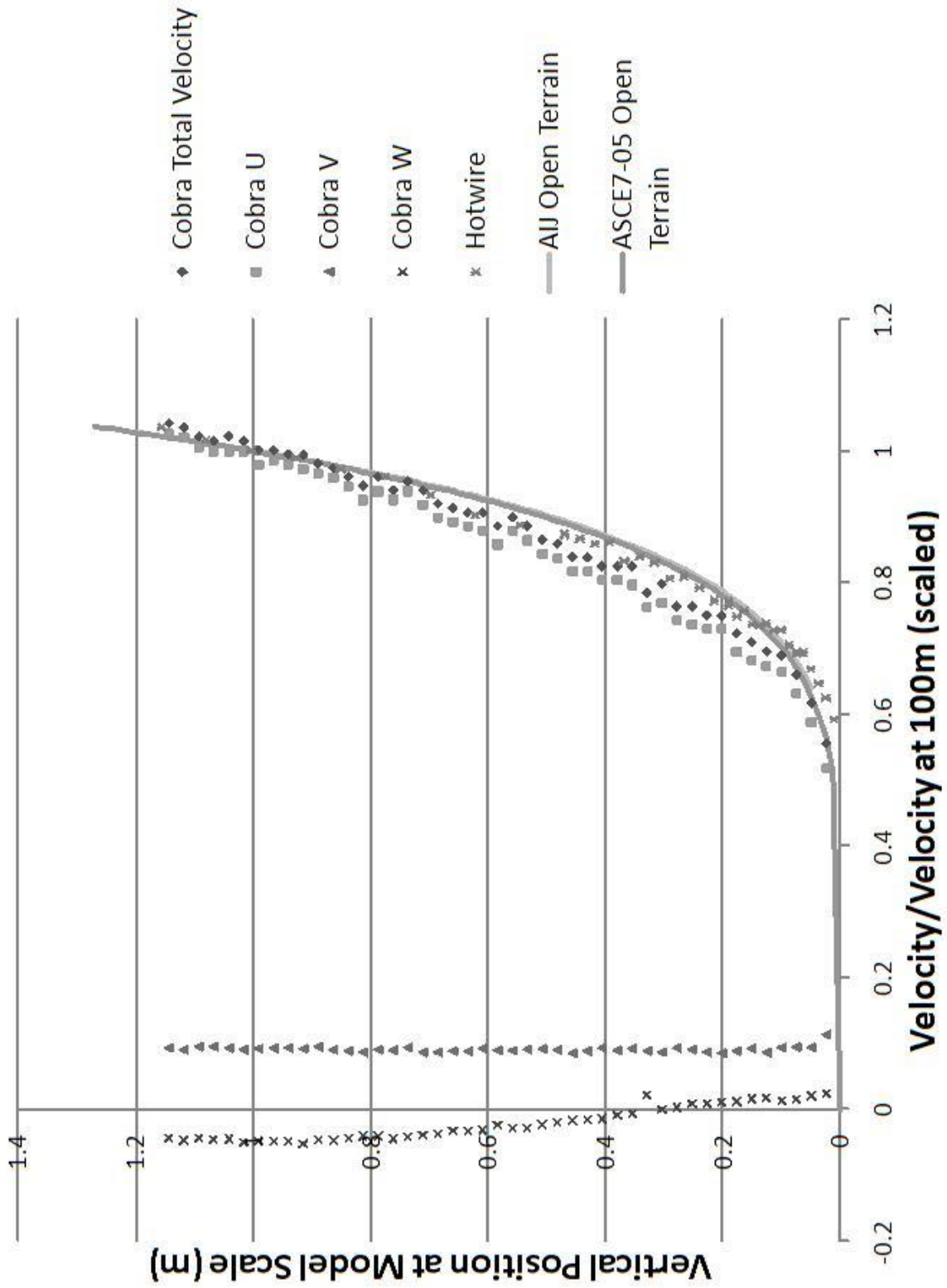
Figure 2.11   Open terrain normalized velocity profile
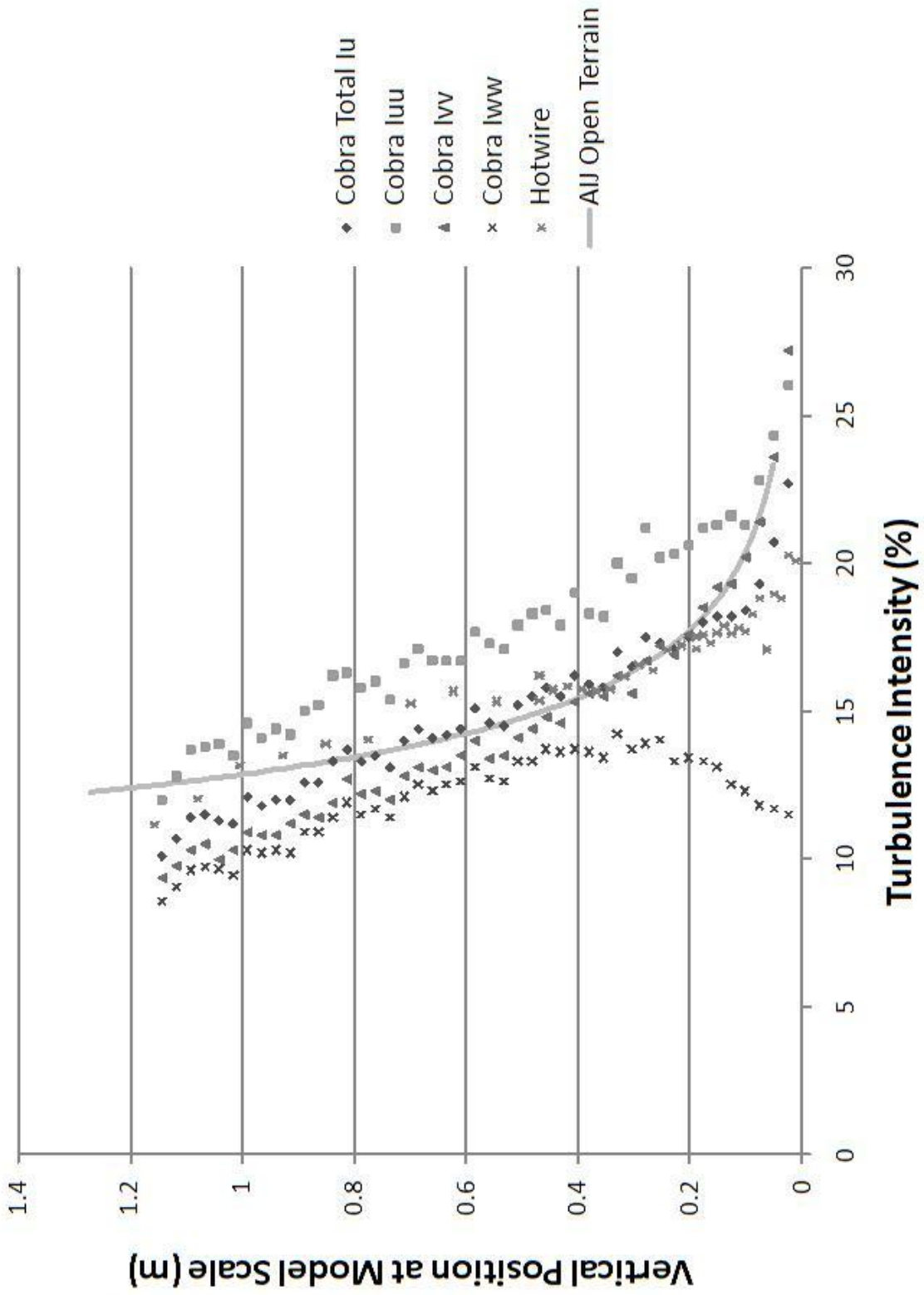
Figure 2.12 Open terrain turbulence intensity profile
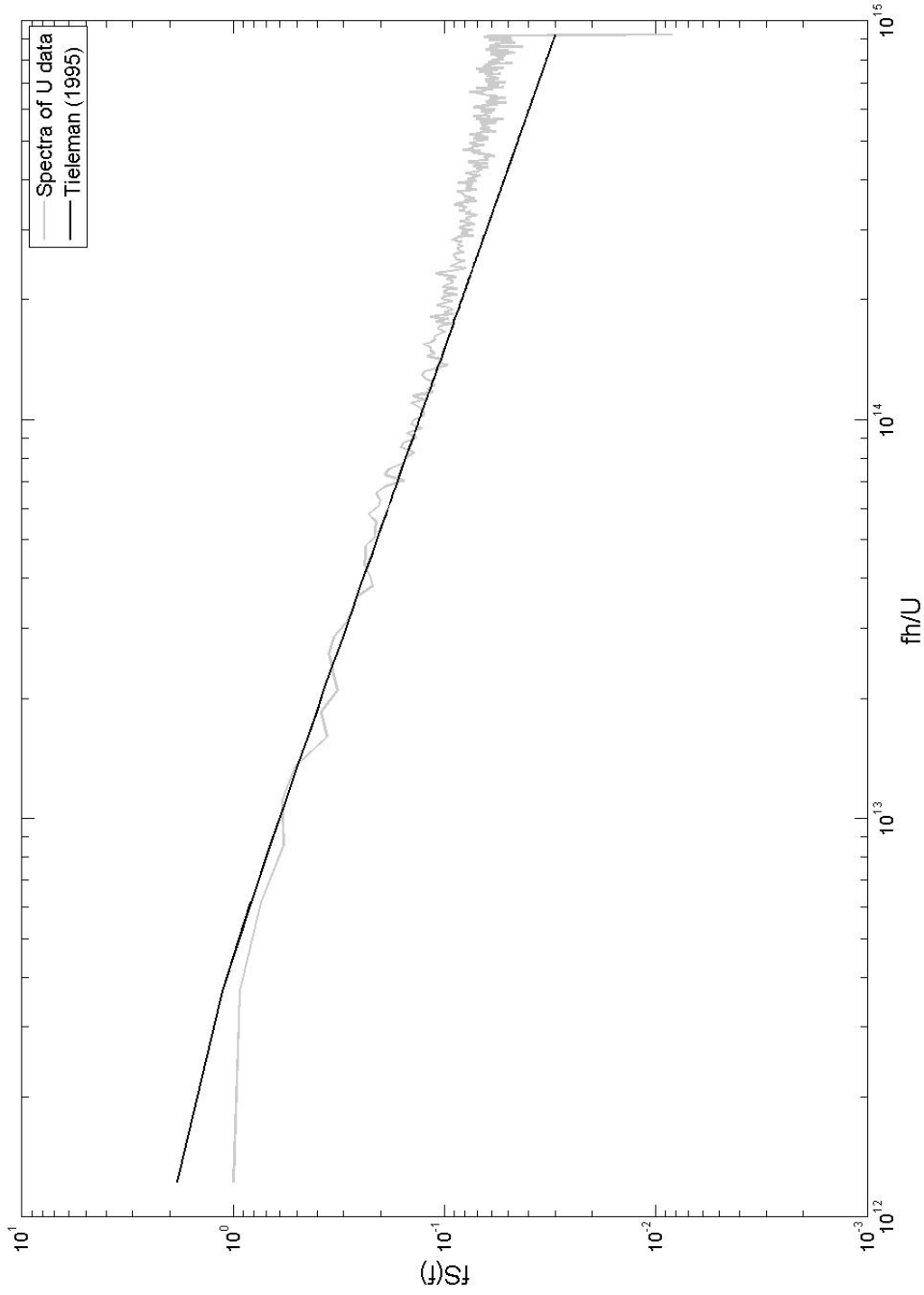
Figure 2.13   Open terrain spectra at 6 cm height
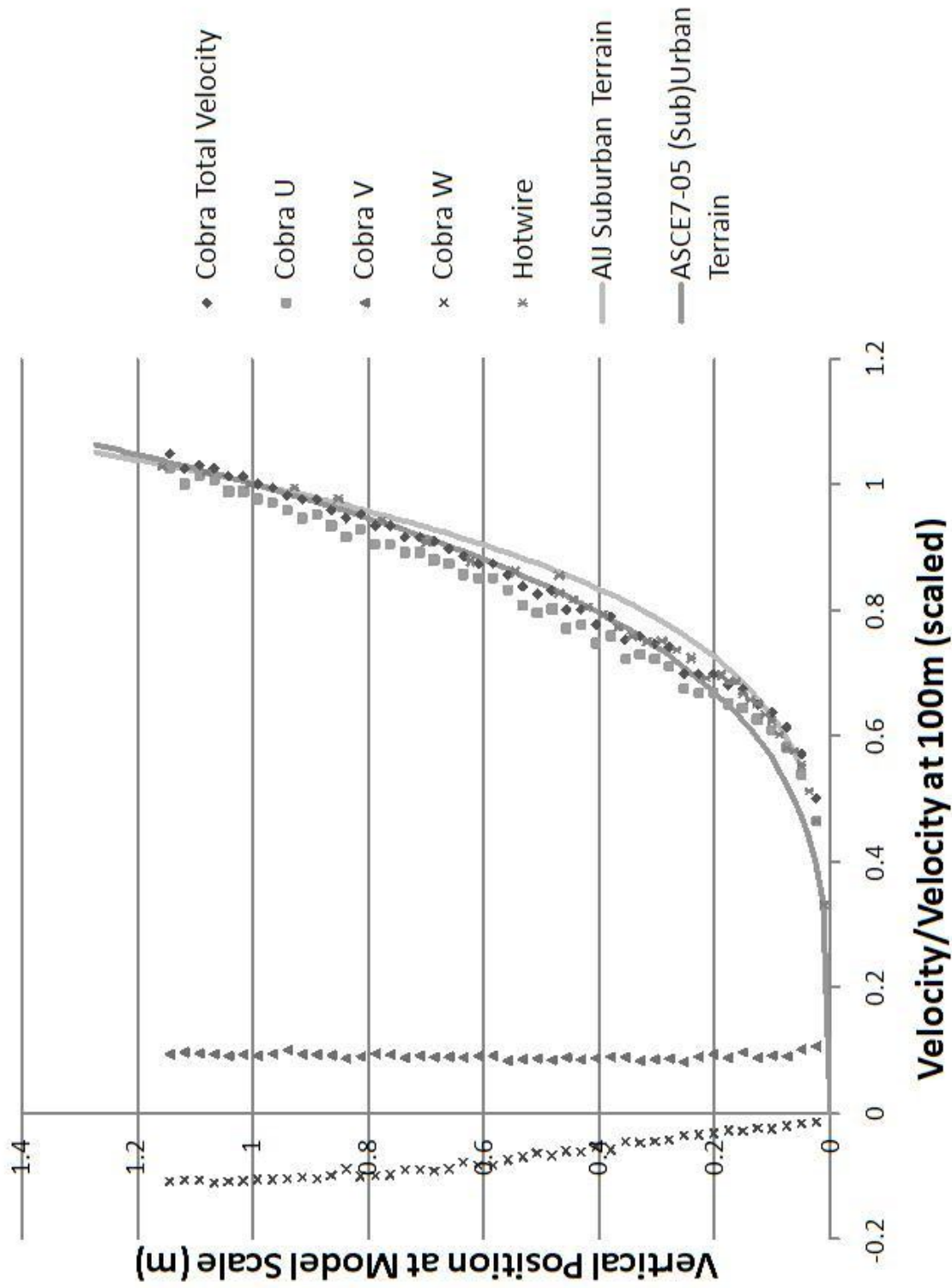
Figure 2.14   Suburban terrain normalized velocity profile
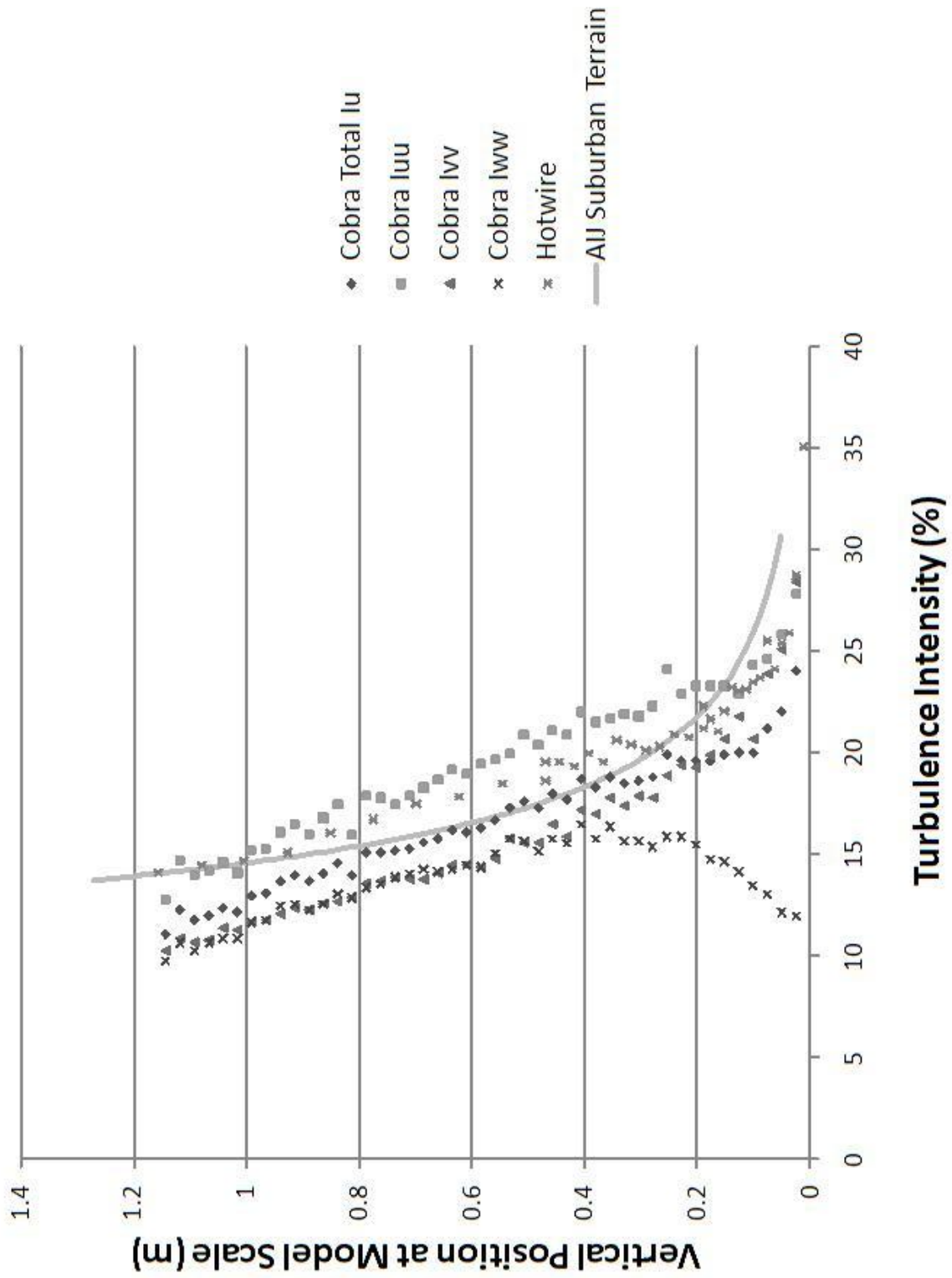
Figure 2.15 Suburban terrain turbulence intensity profile
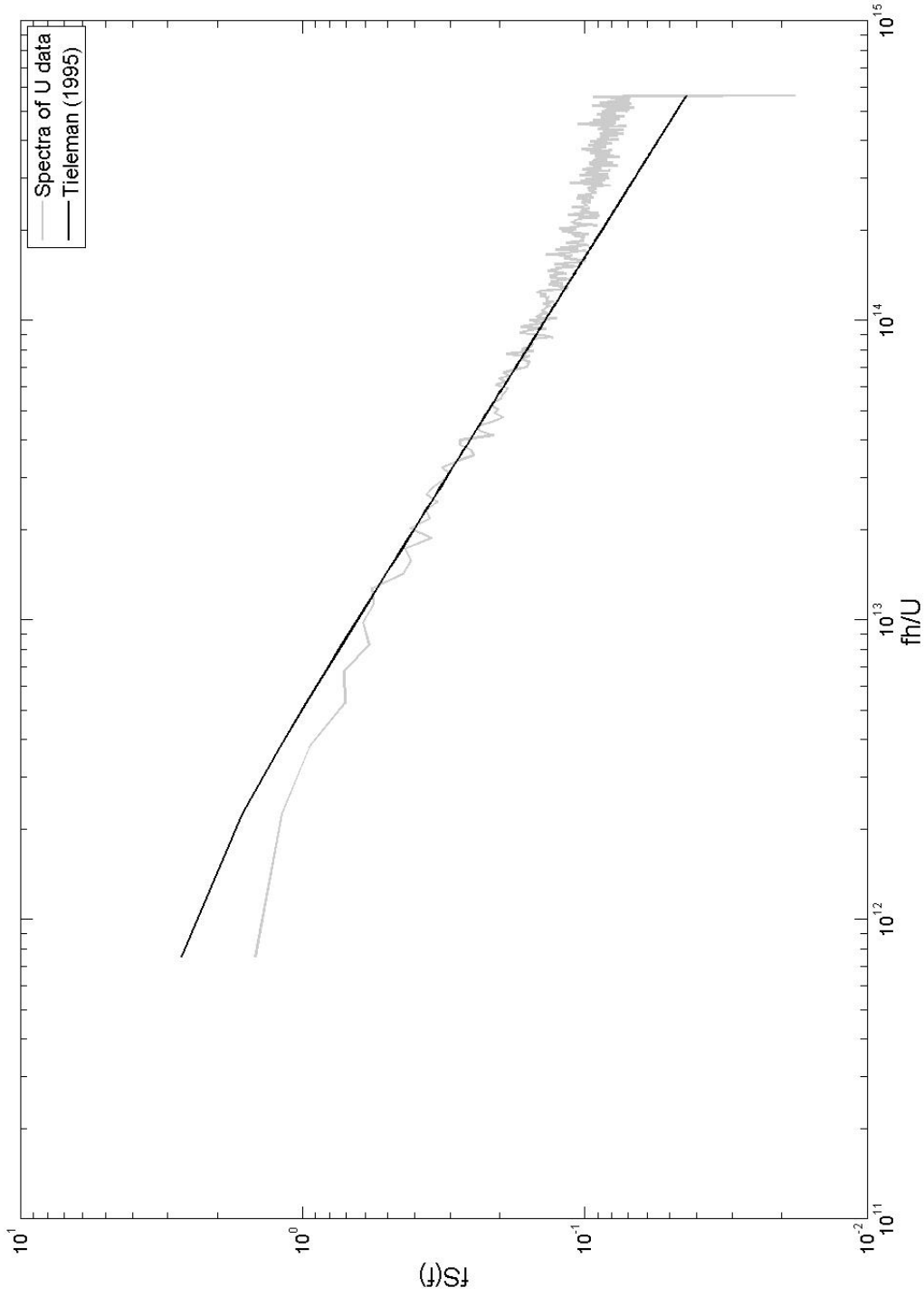
Figure 2.16 Suburban terrain spectra at 6 cm height
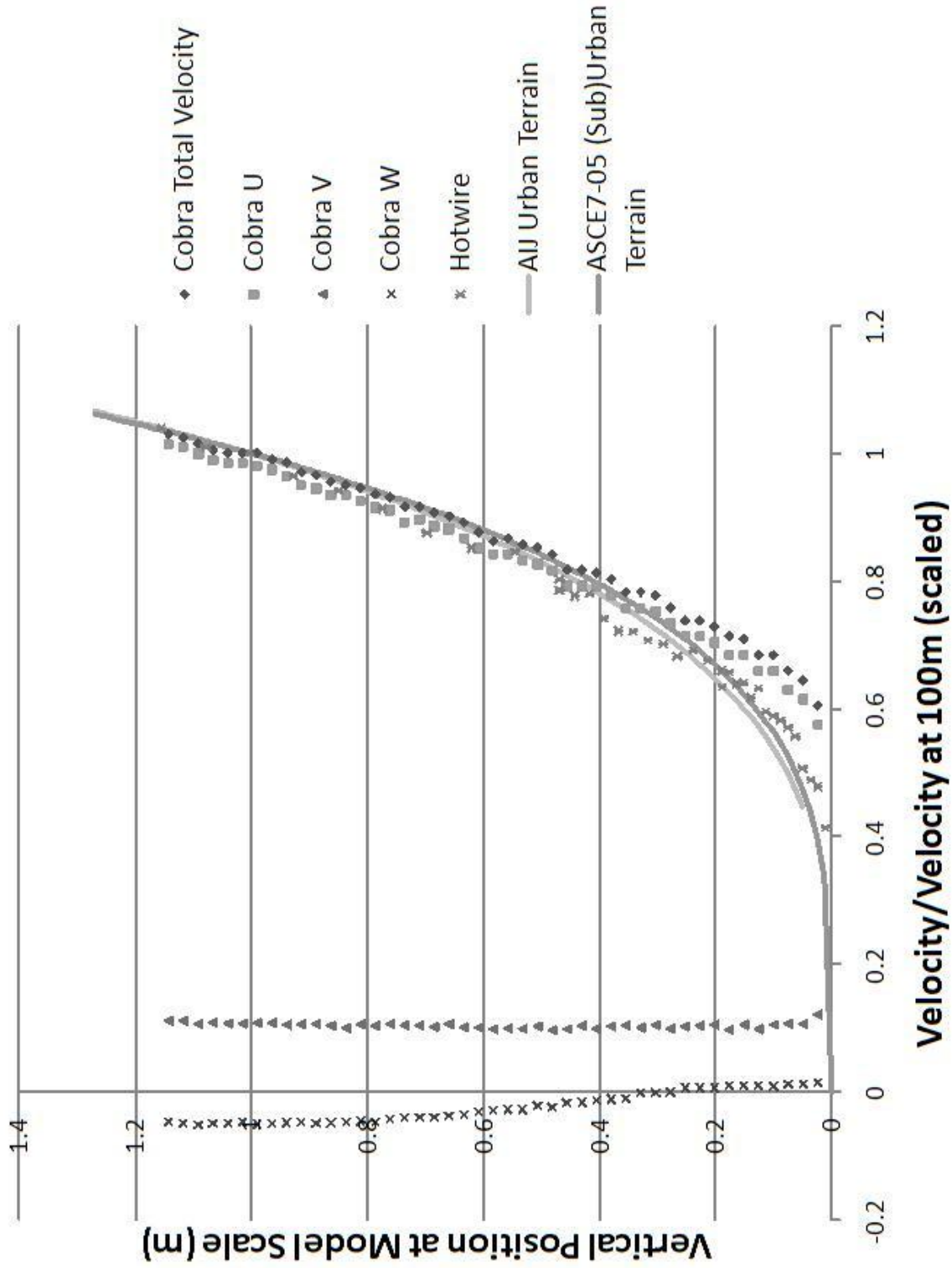
Figure 2.17 Urban terrain normalized velocity profile
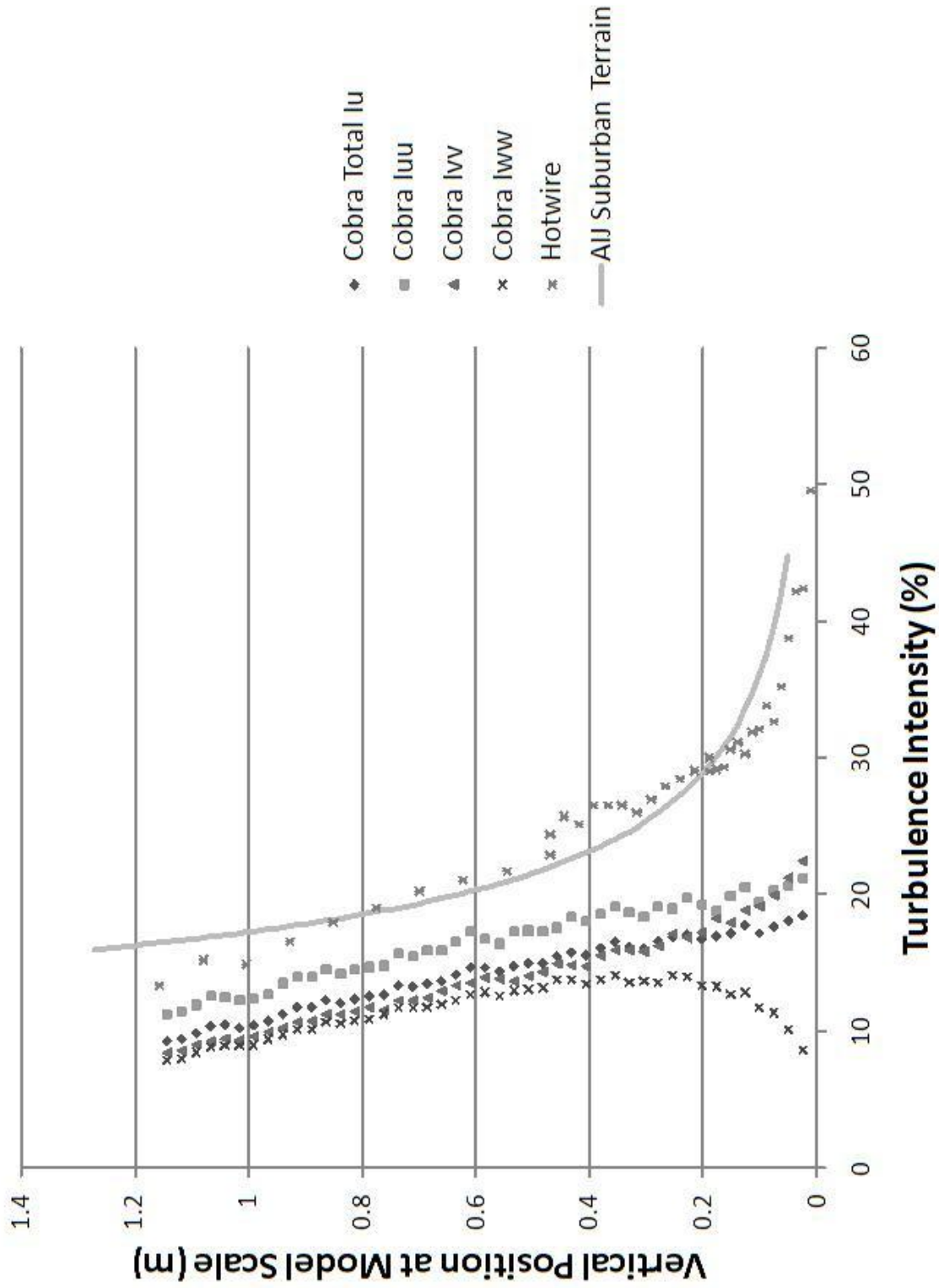
Figure 2.18   Urban terrain turbulence intensity profile
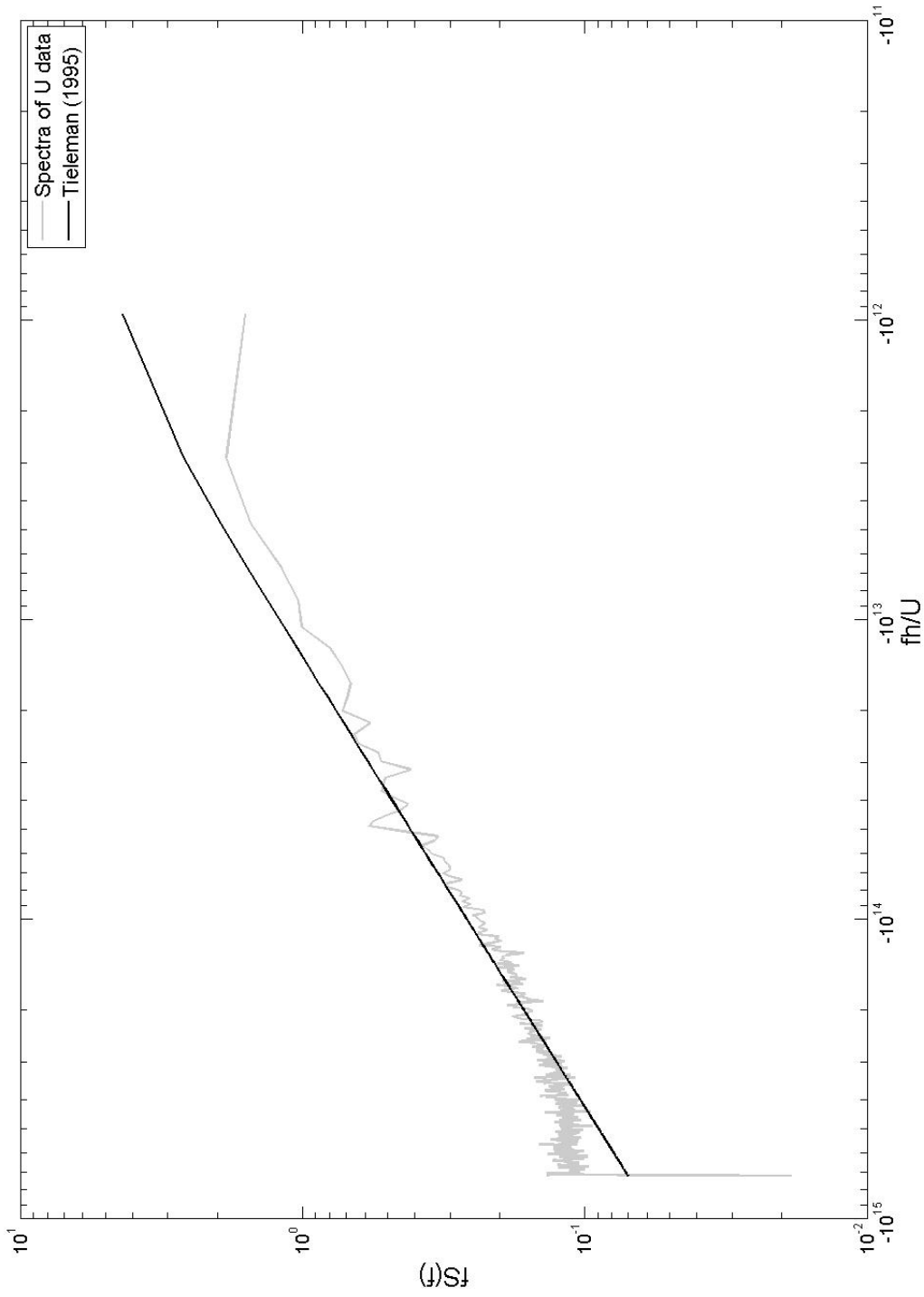
Figure 2.19   Urban terrain spectra at 6 cm height
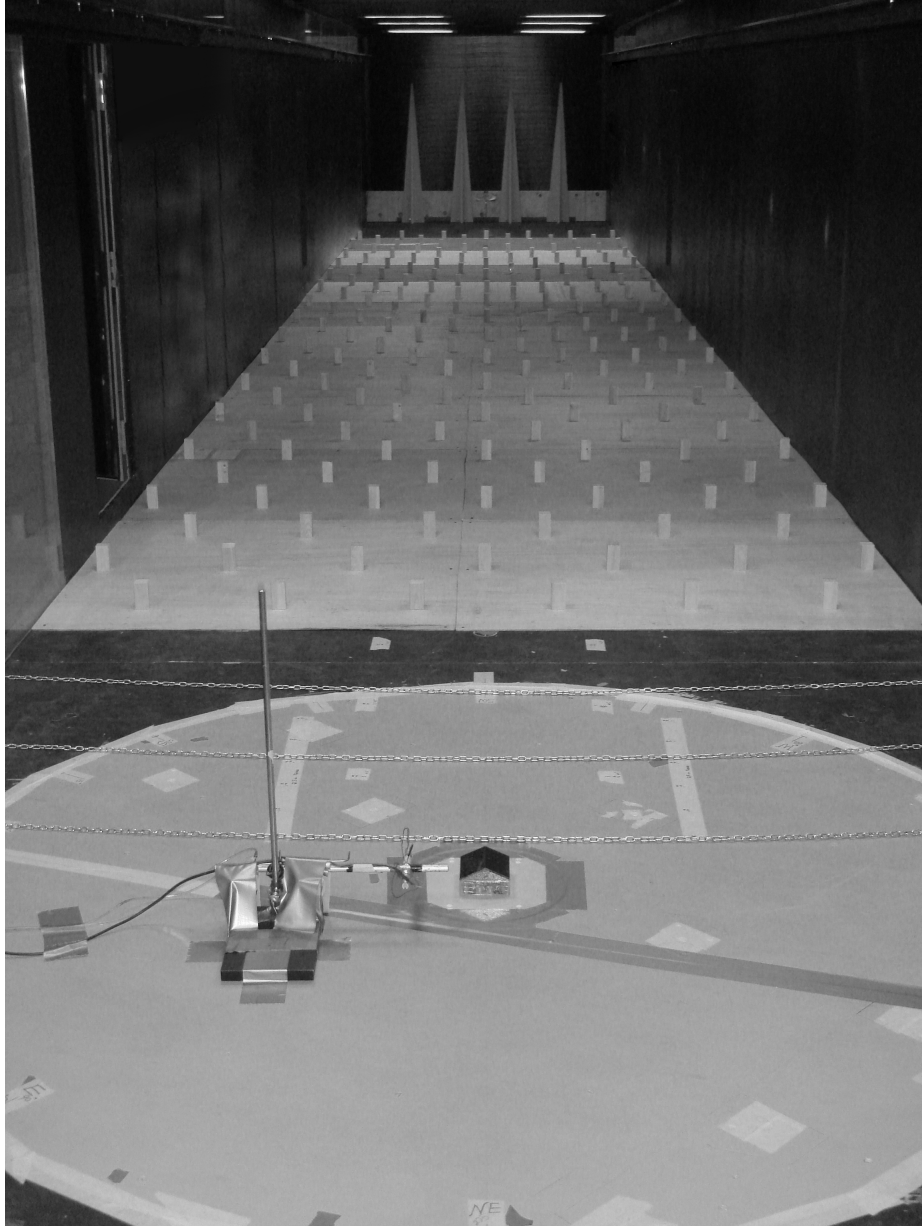
Figure 2.20   Suburban terrain ABL configuration

Table 2.4   Calculated quantities for atmospheric boundary layers

Terrain	Open	Suburban	Urban
Power Law Exponent	0.13	0.2197	0.21
Aerodynamic Roughness Length (mm)	0.021	1.7	0.35
Friction Velocity (m/s)	0.2879	0.4964	0.0058
Friction Coefficient	0.0013	0.0058	0.0036

Table 2.5   Floor roughness used for ABL generation

Terrain	Open	Suburban	Urban
Blocks	None	Block layout A	Block layout B
Chains	29 rows	6 rows	None
Chain row spacing (in)	16.75	11	
Chain to turntable center	37 in	6 in	N/A

Table 2.6   Obstacles used for ABL generation

Terrain	Open	Suburban	Urban
Spire Set	A	E	B
Wall	12 in	12 in	12 in
Ceiling Configuration	Chains	Block	Block
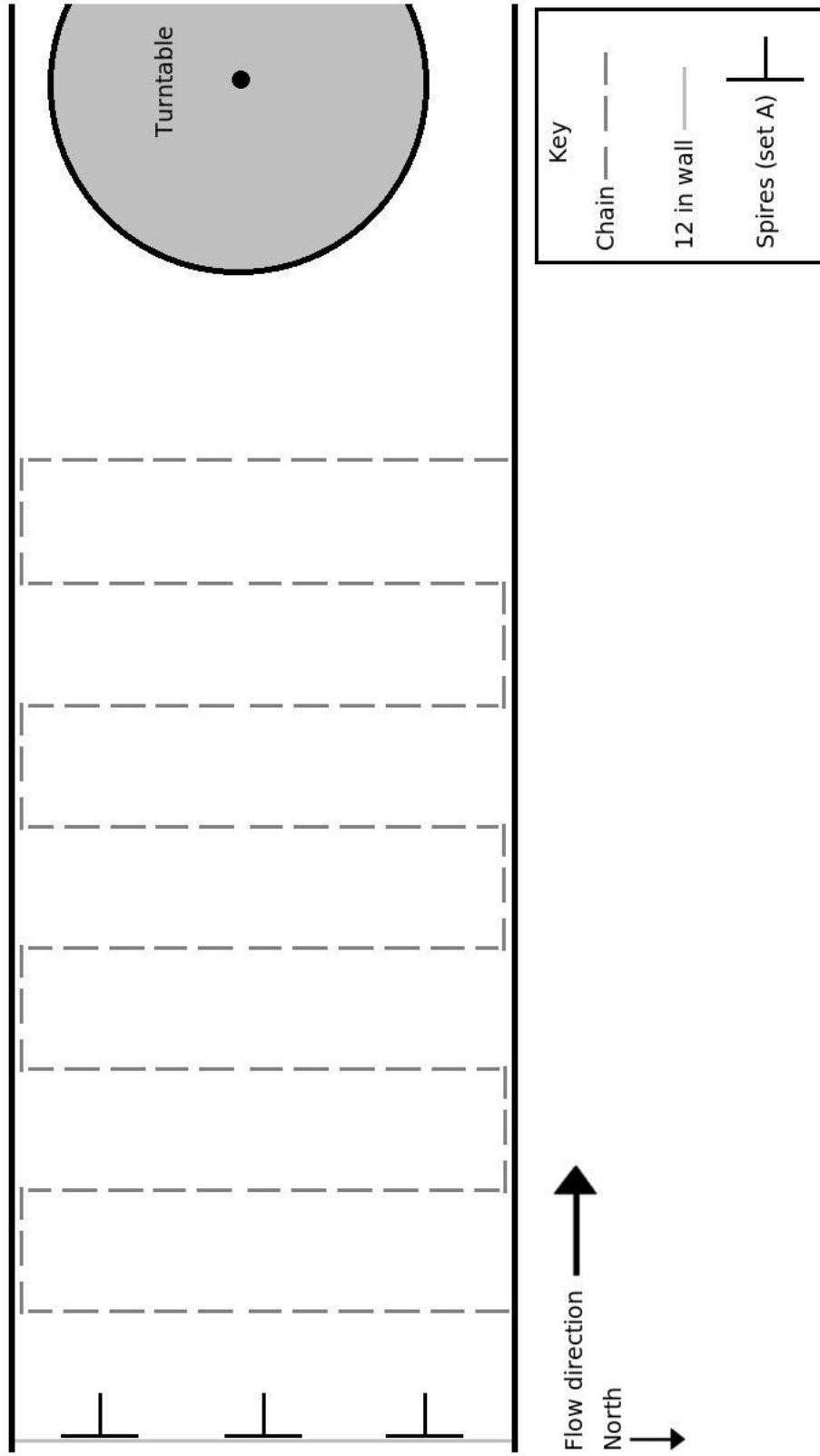
Figure 2.21 Open terrain

36
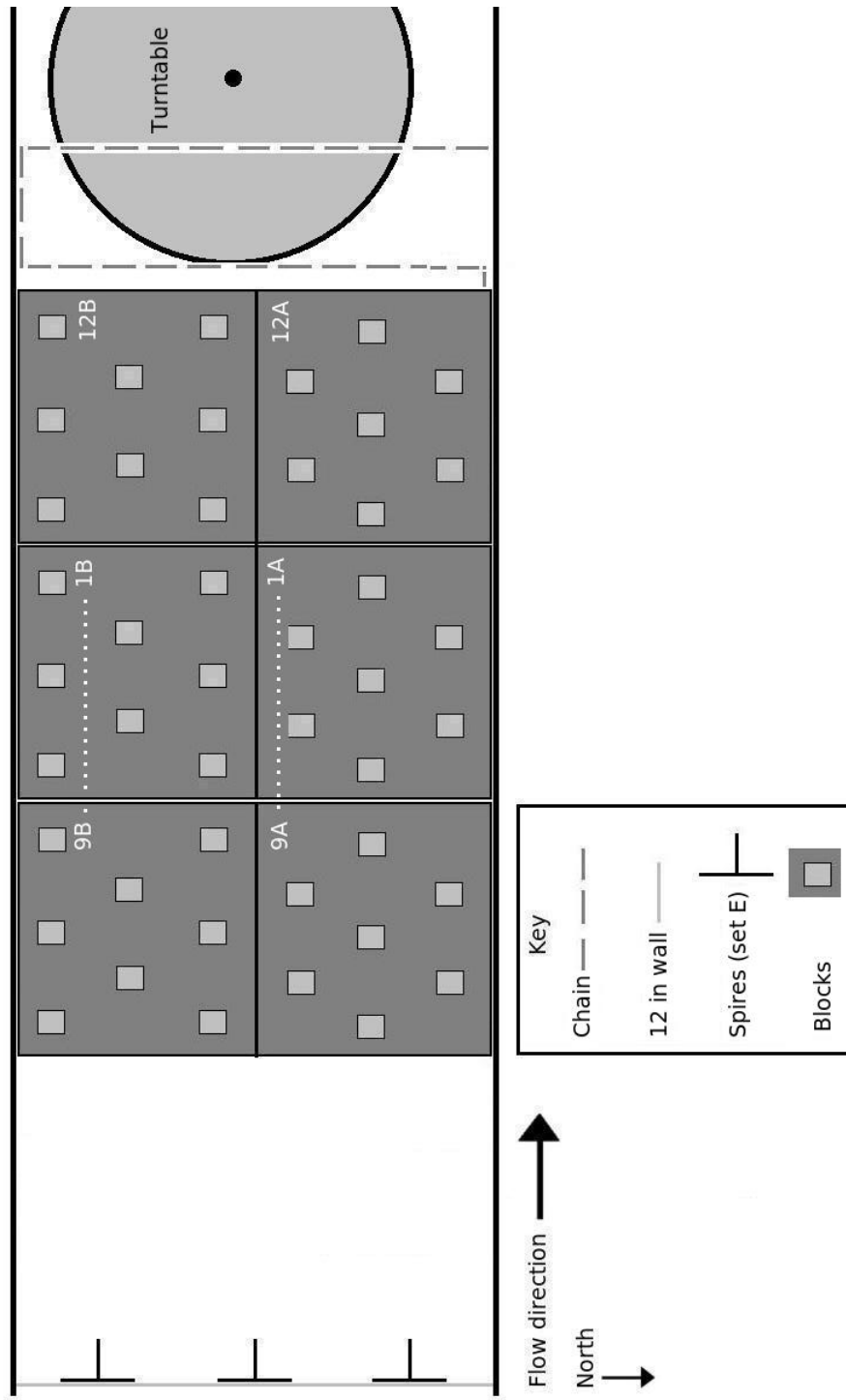
Figure 2.22   Suburban terrain

Turntable

1B

1A

9B

9A

12B

12A

Flow direction

North

Key

12 in wall

Spires (set A)

Blocks
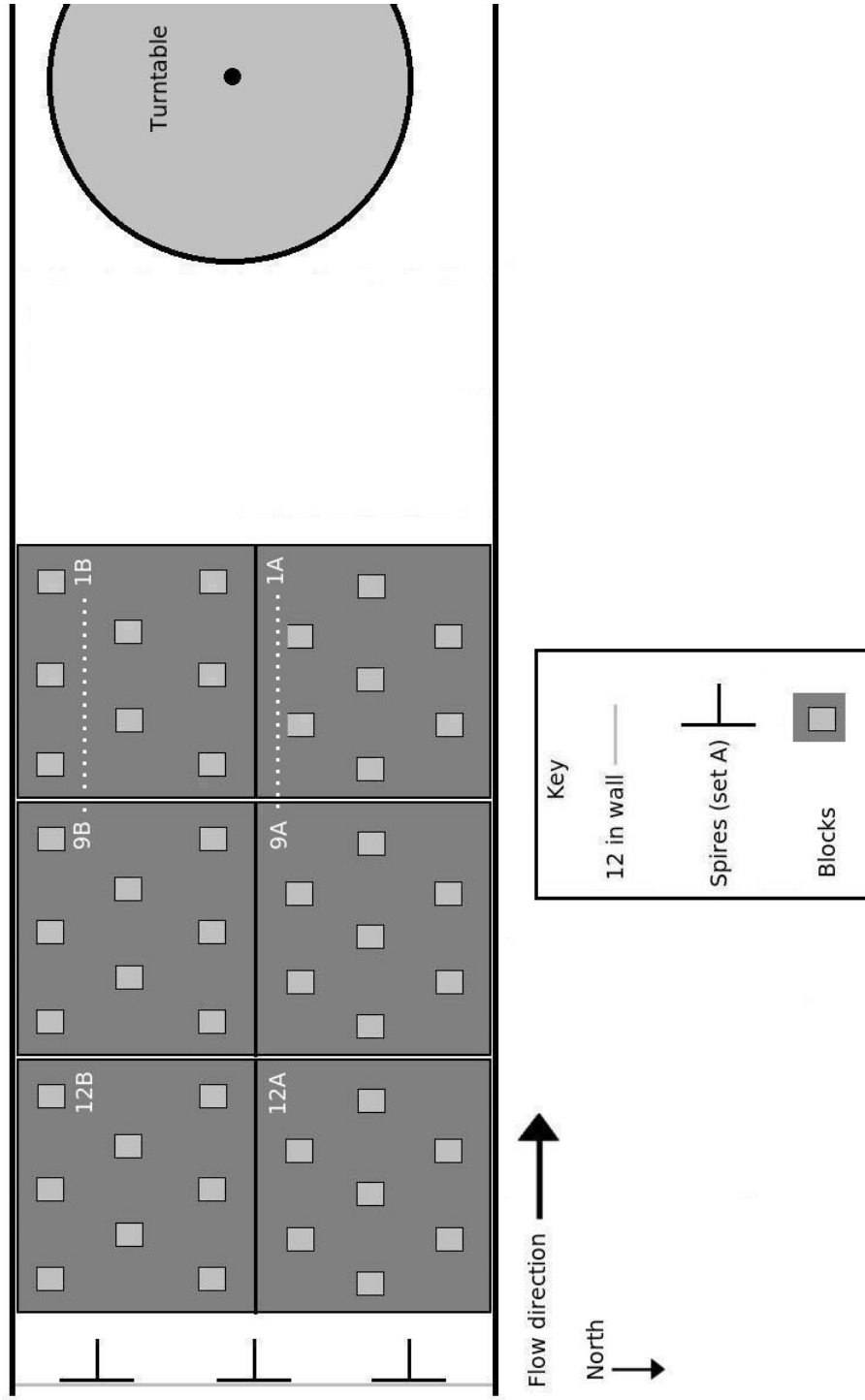
Figure 2.23   Urban terrain

CHAPTER 3.   GUST SIMULATION AND ANALYSIS TECHNIQUES

3.1   Introduction

After developing the atmospheric boundary layers, the effects of gusting were investigated. Gust events were studied because in storms, gust events are common. The lack of previous work on this topic meant the gusting system options had to be evaluated in order to select the gusts to be studied. The goal of this investigation was to produce gusts with as large a velocity change as possible, because extreme gust events would generate the strongest effect on the boundary layer. Two analysis methods were investigated for the gusting data and wavelet analysis was selected as the most effective method.

3.2   Gusting Set-up

Gusts were studied for the three atmospheric boundary layers developed; open terrain, suburban terrain, and urban terrain. Gusts in laminar flow were initially investigated, primarily to determine what gust types would be useful in the boundary layers. For each all of the simulated gusts, there were four parameters used; gust type, mean wind tunnel speed, damper speed, and closing distance (i.e. the distance the dampers moved).

3.2.1   Gusting System

The gusting system in the AABL wind tunnel consists of a bypass duct around the main wind tunnel fan. Damper vanes in the bypass duct control the amount of air that is diverted from the main circuit into the bypass and thus control the velocity in the main circuit's test section. The damper vanes were controlled by a computer, which allowed both detailed programming of the gust event as well as a timing function so the gusts would occur consistently

from one trial to the next. Because this system was new, many calibrating gusts, discussed in the next section, were run to determine the effects of the various parameters. The system was designed to generate gusts with a maximum duration of 5 seconds and a velocity increase of 15%-20% of the mean initial velocity (1). The duration and magnitude of the final gusts selected for study are compared with full scale and wind tunnel scale minimum and maximum gusts (1) in Table 3.1. This table shows that the gusts simulated were within the reasonable range for extreme weather gusts.

The hotwire probe and AA Labs anemometer were used to measure gusts in both the laminar and turbulent flows at a sampling rate of 8600 Hz. The Cobra probe, using a sampling rate of 2500 Hz, was used to measure gusts within the turbulent flows as well. The AABL wind and gust tunnel configurations described previously were used to generate the open, suburban, and urban terrain boundary layers, and the wind tunnel roof was adjusted to provide a zero pressure gradient.

3.2.2 Parameter Calibration

3.2.2.1 Gust Events

For this study, two types of gust events were investigated. The first gust event (Gust A) was a sudden increase in wind tunnel velocity, as shown in Figure 3.1. Gust A was generated by closing the dampers after data collection began, and leaving them closed until the test was over. The second type of gust event (Gust B) was a sudden increase in wind tunnel velocity followed by an immediate decrease. Gust B was generated by closing the dampers after data collection began and immediately returning them to a fully open position. Because Gust B did not attain as large a velocity change as Gust A, Gust A was thought to have more potential in displaying a measurable change in the ABL during the gust event.

3.2.2.2 Event Parameters

Mean wind tunnel speed, damper speed, and closing distance were varied for both gust types. This data was taken before the development of the Labview trigger program, so the

gusts were not consistently timed throughout the tests. These tests, in fact, made the need for a program to trigger both data collection and then the gust event very clear. Figure 3.2 displays the effect of changing the mean wind tunnel velocity for Gust A, with a closing distance of 48,000 steps and a damper speed of 50,000 steps/s. Although the gusts were not activated at a consistent time within the tests, it is still apparent that the faster mean wind tunnel speed produces The intuitive effect of damper speed, as seen in Figure 3.3 was to decrease the velocity rise time as the damper speed increased. The closing distance also had a predictable effect, as Figure 3.4 shows that the largest closing distance produced the largest velocity increase. In order to generate the most dramatic results, the final tests were all performed with the maximum closing distance of 48,000 steps. The damper speeds and mean wind tunnel speeds were varied between the hotwire tests and Cobra tests.

3.3 Final Gust Tests

In order to take advantage of statistical analysis, each gust case was run ten times. For the smooth flow, the ten trials were ensemble averaged in order to reduce the noise in the data. Figures 3.1 through 3.4 all display smooth flow data.

3.3.1 Hotwire Tests

The hotwire tests were performed in the same manner as the parameter tests, although with the triggering system in place. Because the shutter speed of 50,000 steps/s was indistinguishable from the shutter speed of 100,000 steps/s it was replaced by a speed of 30,000 steps/s. The mean wind tunnel speed of 5 m/s was discarded because the velocity increase was so small. The hotwire was suspended from a stand in the center of the test section. The smooth flow data from the hotwire tests were used to calculate the gust durations and accelerations, which are listed in Table 3.1, where both the gust duration and acceleration refer to the increasing velocity, so for gust type B, the time of the peak of the gust was used. The gust naming convention includes the gust type, A or B, and the damper closing speed in thousands of steps per second. For example, gust A30 refers to a type A gust with a damper closing speed of 30,000 steps/s.

Table 3.1   Gust Characteristics

Gust Type	Duration (s)	Magnitude (% of initial velocity)	Acceleration (m/s/s)
A10	9.06	31.9	0.52
A30	6.16	30.6	0.74
A100	5.8	31.7	0.83
B10	6.03	26.8	0.66
B30	2.35	18.2	1.15
B100	0.8	9.7	1.88
Full Scale Min	-	-	0.04
Full Scale Max	-	-	0.4
Simulated Min	-	-	0.2
Simulated Max	-	-	20

3.3.2   Cobra Probe Tests

After the initial analysis of the hotwire data was complete, some parameters were changed for the Cobra probe tests, in order to generate more extreme gust events. The shutter speed of 10,000 steps/s was replaced with 150,000 steps/s, and the mean wind tunnel velocities used were 15 and 20 m/s. The Cobra probe tests were performed at three heights above the floor; 6cm, 10cm, and 50cm. The Cobra probe was mounted on the traverse for the 50cm tests, but to reduce shaking it was suspended from a stand for the other heights. The tests were run for 10 seconds, in order to allow ample time for the velocity to settle after the gust event. Additionally, some tests at the higher speeds were eliminated due to the stress they were imposing on the wind tunnel near the fan.
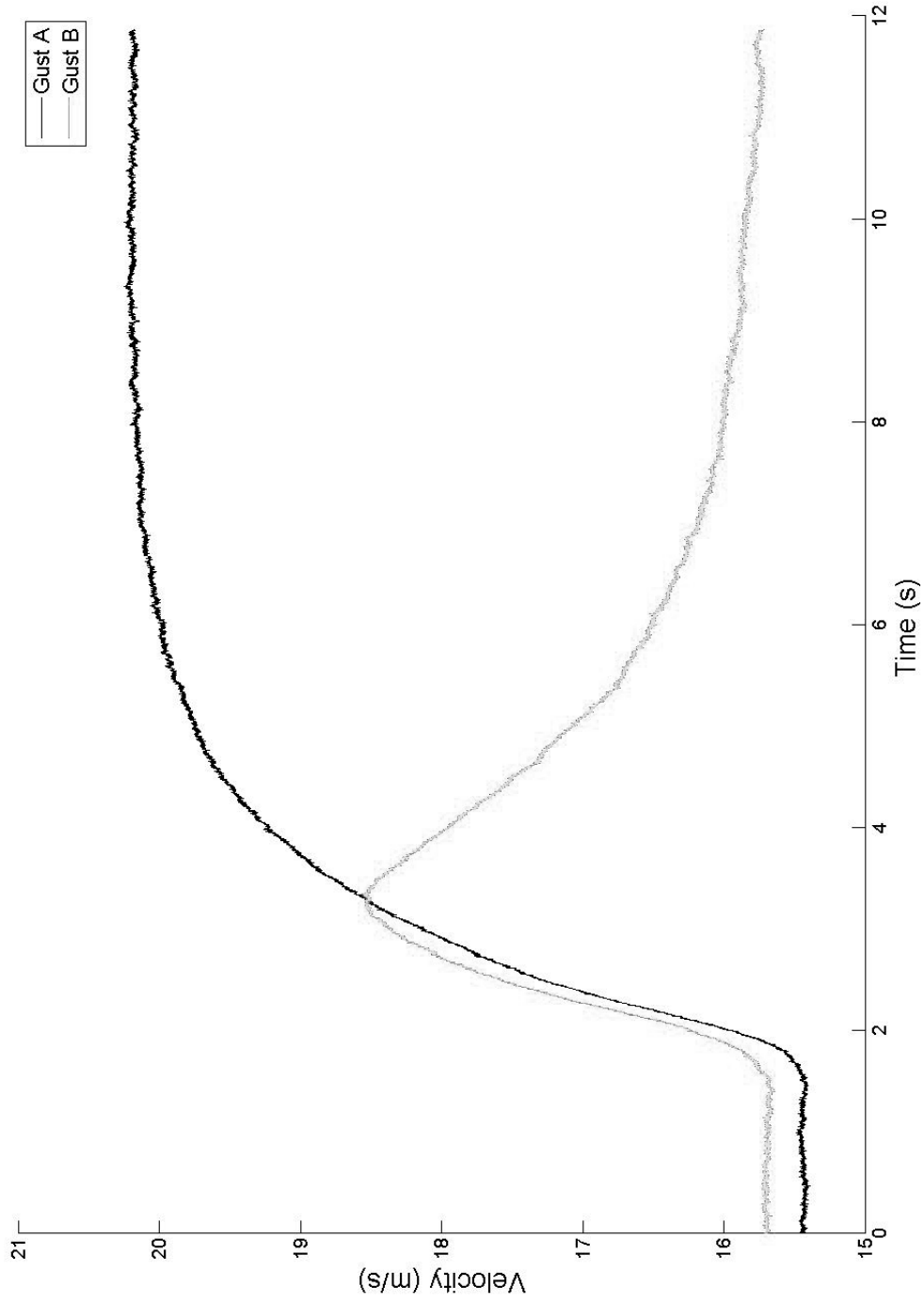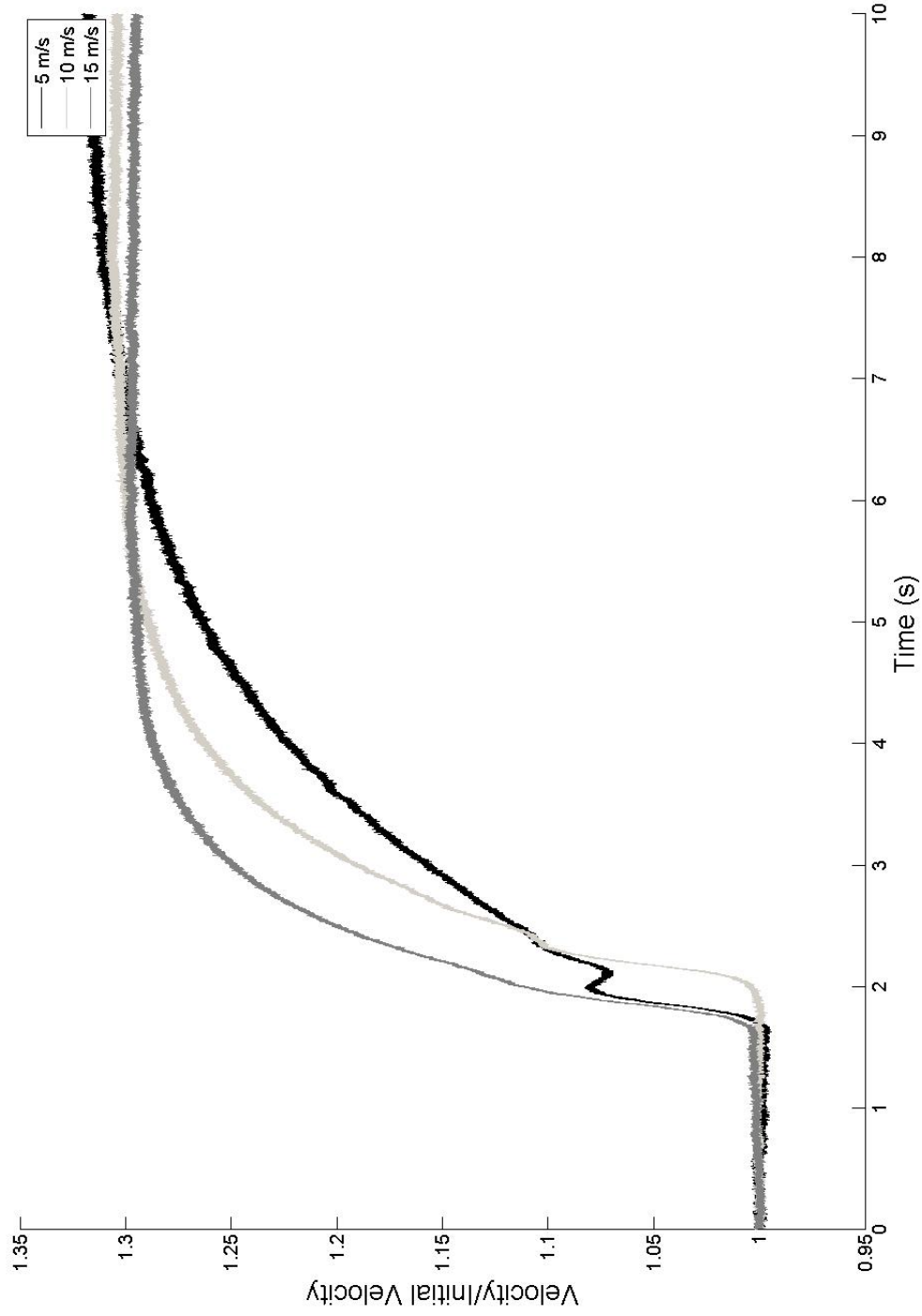
Figure 3.1 Gust Types

Figure 3.2   Effects of mean wind tunnel velocity
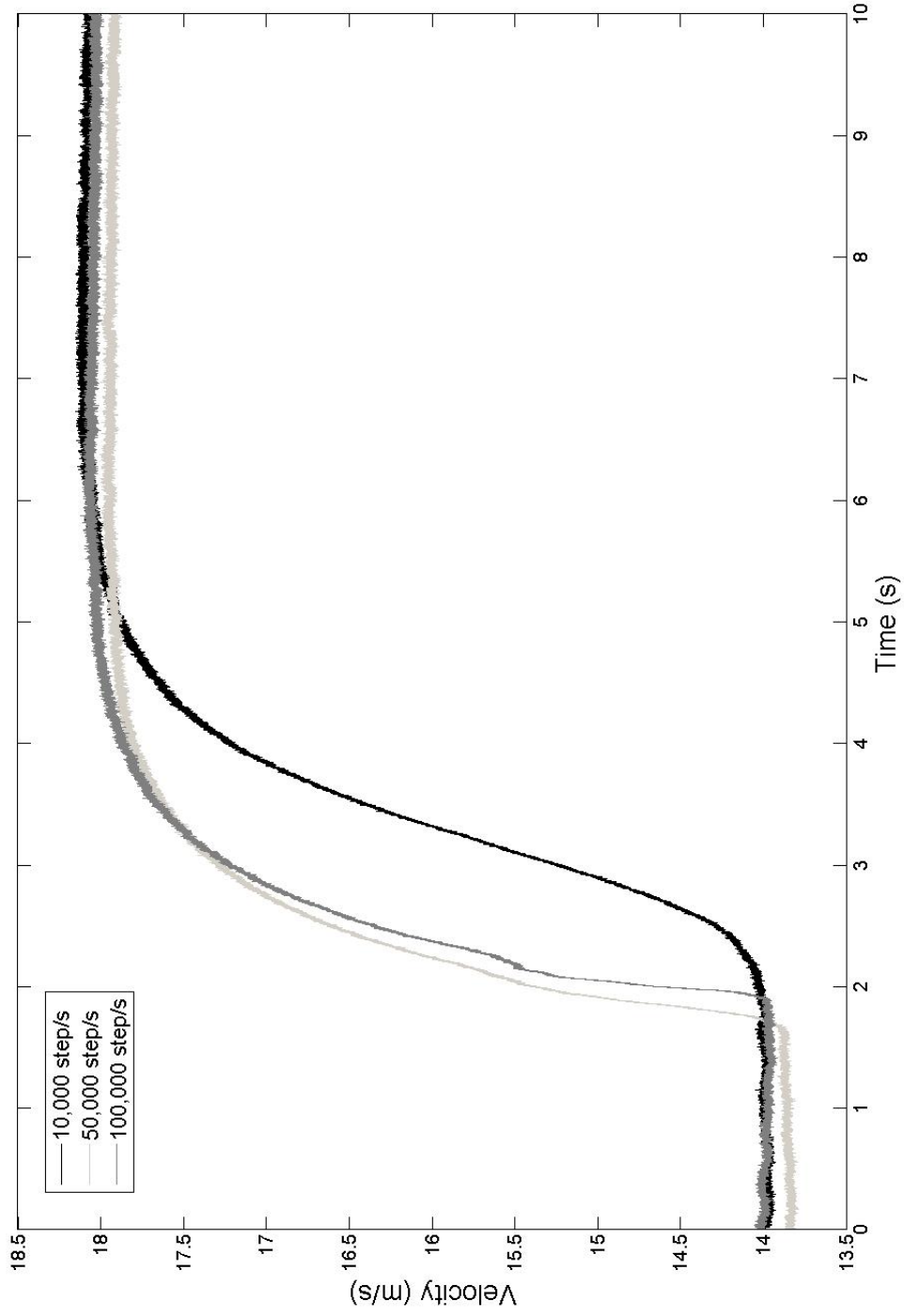
Figure 3.3   Effects of damper closing speed
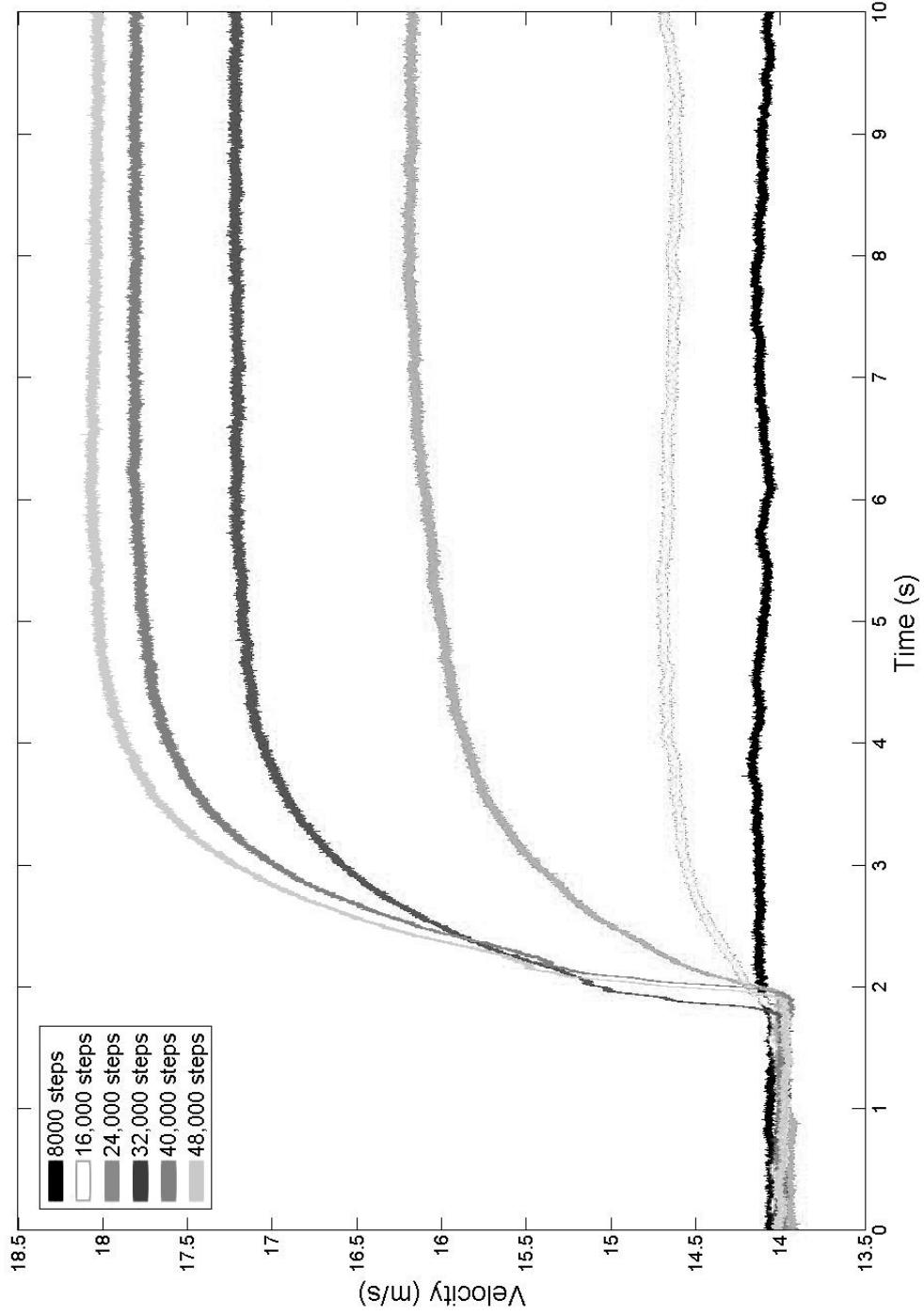
Figure 3.4   Effects of damper closing distance

3.4 Analysis Techniques

The smooth gusting tests established the changes that occur in mean velocity with a gust event. While in the atmospheric boundary layers high levels of turbulence intensity conceal and perhaps partially dissipate these mean velocity changes, it seemed more useful to study the effect the gust had on the turbulence intensity. However, turbulence intensity is a statistical quantity, so there was no simplistic way to determine the effect of a non-stationary gust such as this. A power spectral density function could not be calculated from the data runs because the mean of the data varied with time. A Fourier transform of data with a time varying mean is meaningless, because the mean must be subtracted out in order to study the deviations from it. Thus, two other methods were used to analyze the ABL gusting data. A turbulence intensity time series was calculated, but wavelets were primarily used for analysis, as they provide a more rigorous time-frequency analysis.

3.4.1 Time-varying Turbulence Intensity

The turbulence intensity time series in each direction were calculated from the **U**, **V**, and **W** velocity vectors measured by the Cobra probe. A sliding window of twenty points was used in MATLAB to find mean and root mean square (RMS) values around every velocity point, excepting the ten points on each end of the vector. The code developed is available in Appendix A. The turbulence intensity was calculated by dividing the calculated RMS by the corresponding calculated mean for each point, and plotted, as in Figure 3.5. Equations 3.1 through 3.3 were used, with i varying over the entire velocity vector.

Mean Velocity

$$meanvelocity_i = \frac{1}{20} \sum_{j=i-10}^{i+10} V_i \tag{3.1}$$

Root Mean Square

$$RMS_i = \sqrt{\frac{1}{20} \sum_{j=i-10}^{i+10} V_i^2} \tag{3.2}$$

Turbulence Intensity

$$Iu_i = \frac{RMS_i}{meanvelocity_i} \tag{3.3}$$

This represents an instantaneous turbulence intensity. While the calculated turbulence intensity time series did demonstrate that the turbulence intensity was largest in the **U** direction, there were no noticeable trends in the turbulence intensity correlated to the gust event. If the gust event made an impact upon the turbulence intensity, a change in the turbulence intensity would be expected between 1 and 2 seconds, when the gust occurred. As this method is not mathematically rigorous, it was used primarily as a check of the wavelet analysis.

3.4.2 Wavelets

Wavelets are similar to Fourier transforms, in that they expand a time series (or signal) using transformations of a base function. In the Fourier transform, the base function is an infinite sinusoid, whereas there are many different finite wavelet functions (16). The finite structure of the wavelet base allows the wavelet to generate resolution of a time series in both time and frequency, capturing localized events. A wavelet analysis generates a series of coefficients that describe the signal. Additionally, correlations between signals can be easily discerned with wavelets, by multiplying their coefficients together and plotting them (17). The Morlet wavelet, shown in Figure 3.6, was selected for this analysis, as it had similar shape to the features in the velocity time series (18) and because it is commonly used for turbulent wind analysis (19; 20). The equations for the continuous wavelet transform (16; 20) and the Morlet wavelet (16; 20) are given below, along with the continuous wavelet transform command in MATLAB used to analyze the data. The wavelet transform decomposes the signal, x, using dilation and translation of the selected wavelet function, g, where dilation is performed by the variable a, which is related to frequency (16; 18; 20). In the MATLAB command, *ucoefs* was the name of the output variable, *'u'* was the input variable, *1:128* represents the scales selected for analysis, *morl* signifies the Morlet wavelet, and *glbabs* describes the coefficient plot coloration.

Wavelet Transform

$$W(a,t) = \frac{1}{\sqrt{a}} \int_{-\infty}^{\infty} x(\tau) g(\frac{t-\tau}{a}) d\tau \tag{3.4}$$

Morlet Wavelet

$$g(t) = e^{\frac{-t^2}{2}}(cos(\omega_0 t) + isin(\omega_0 t)) \tag{3.5}$$

MATLAB Transform ucoefs = cwt(u,1:128,'morl','glbabs')

Figure 3.7 displays the typical output of wavelet analysis, as a three dimensional map. While all the results in Chapter 4 are presented as two dimensional figures, which are effectively the top (looking down) view of the three dimensional map, this image makes it easier to understand the wavelet analysis. The curves in the "scales a - COEFS" plane can be considered analogous to a power spectral density function at a particular time. The "scales a" axis is related to frequency. The coloration used corresponds to the "COEFS" axis, and the same coloration is used in the two dimensional wavelet displays to signify the magnitude of the coefficients. The large peaks on the time-scale ends in Figure 3.7 are due to end effects, described in (19).
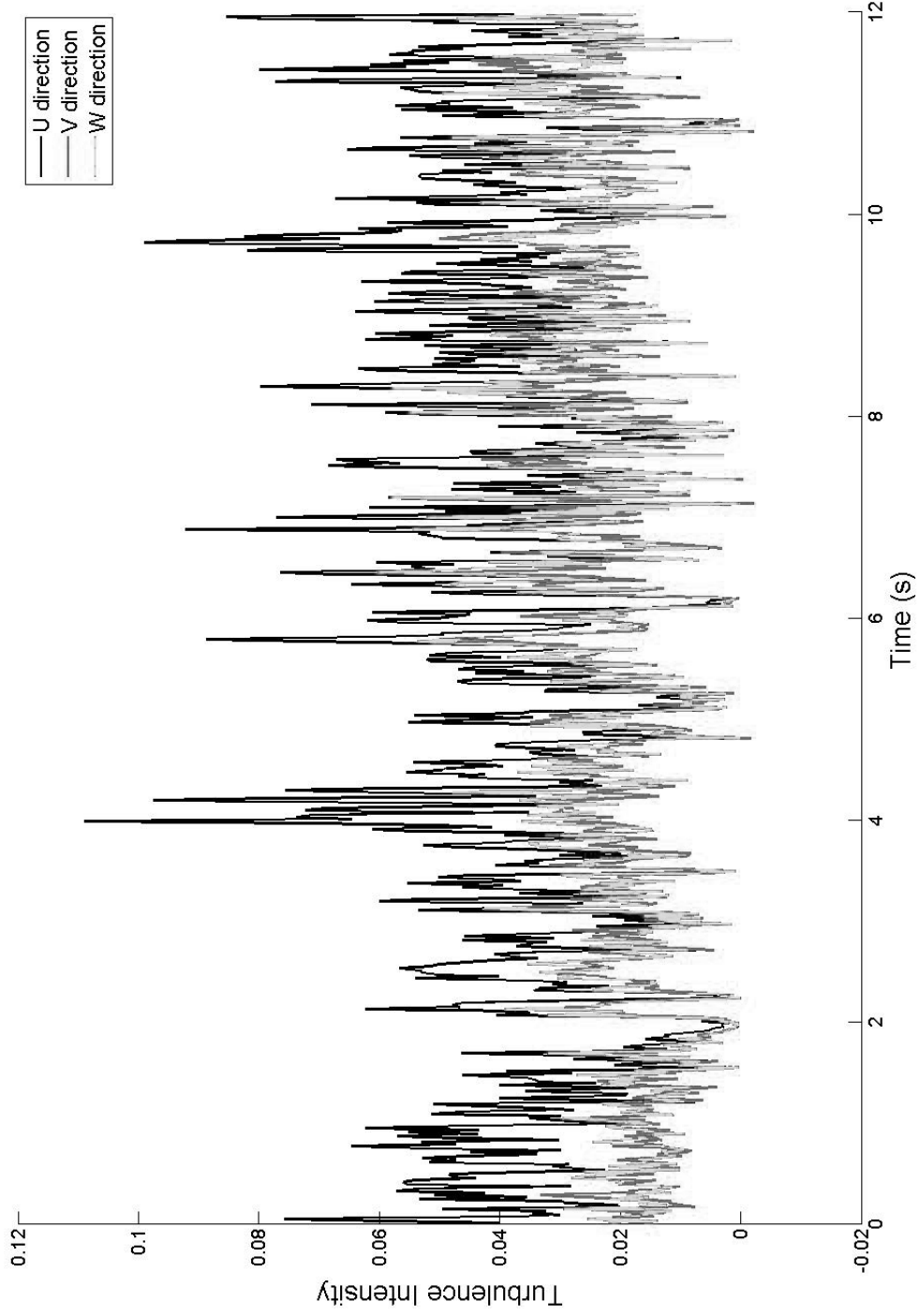
Figure 3.5 Calculated Turbulence Intensity for Suburban Terrain Type A
Gust Event
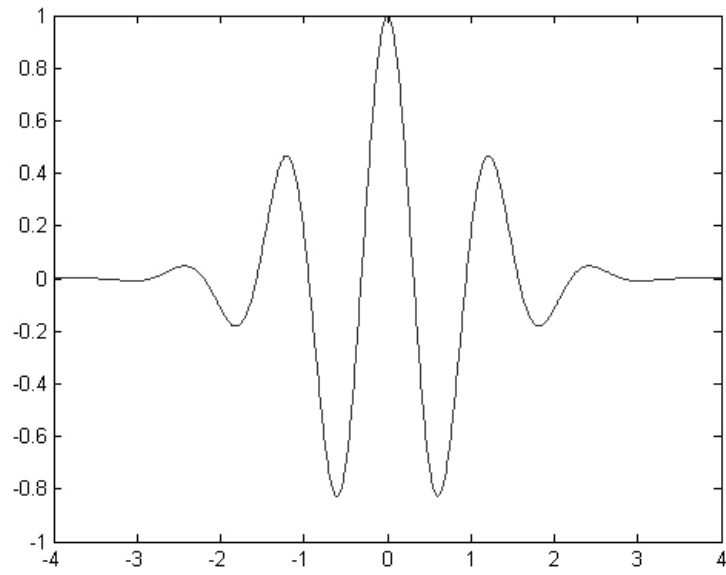
Figure 3.6   Morlet wavelet
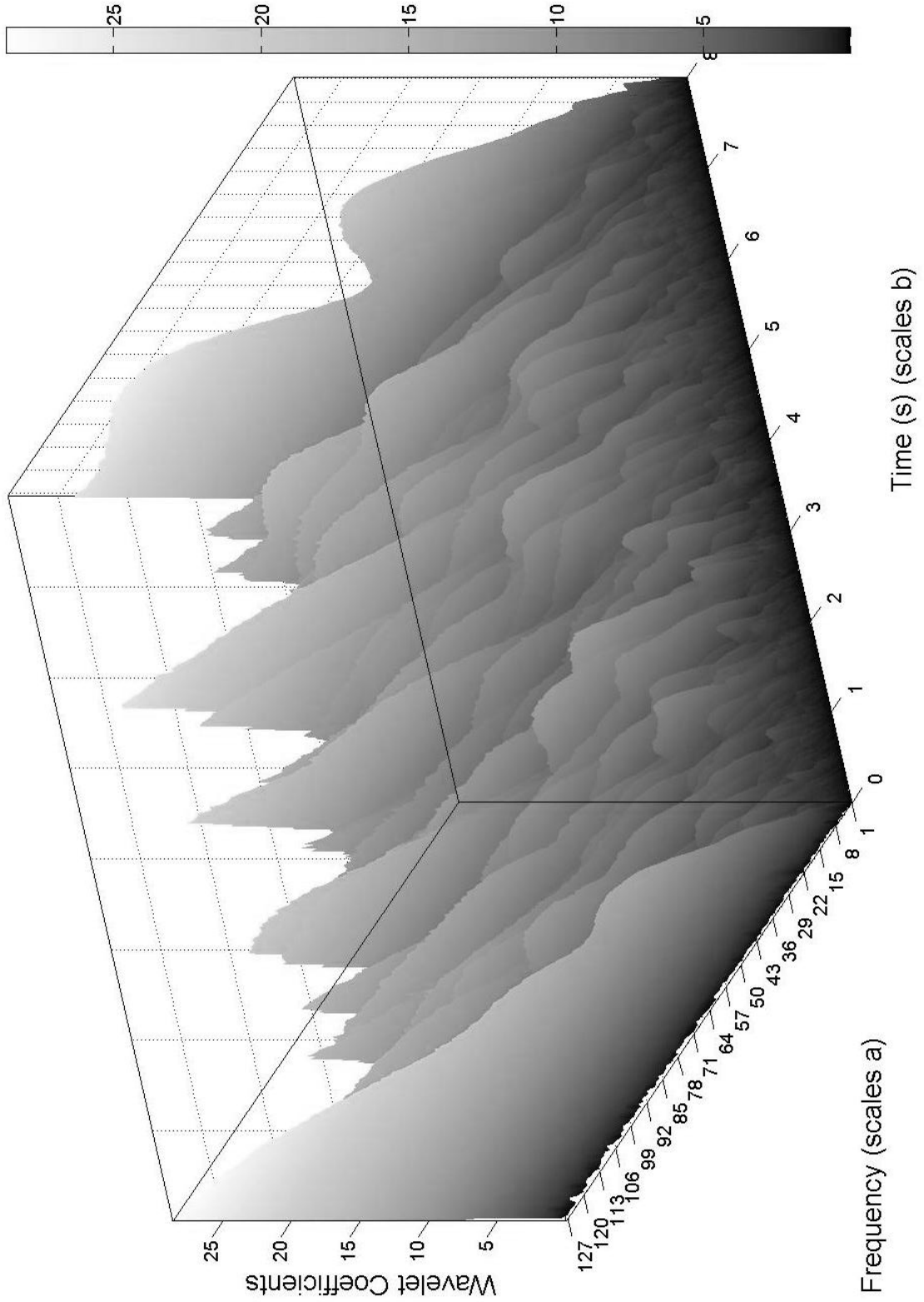
Figure 3.7   Example of wavelet analysis in 3-D display

CHAPTER 4.   GUST RESULTS

4.1   Introduction

Wavelet analysis was used exclusively for the final data analysis, although the time-varying turbulence intensity method was used as a check on the results. Velocity and Reynolds stress were analyzed with the wavelets, leading to the observation that the two gust events explored had no noticeable effect on the atmospheric boundary layer for any of the terrains modeled. The wavelet coefficient maps displayed in this section are only a sampling of all the gust trials analyzed, but they are representative of the entirety of the data. The gusts selected for this section were generated using a variety of parameter settings, which are listed in Table 4.1.

Table 4.1   Gust parameters used in Figures 4.2 through 4.8

Figure	Gust Type	Flow Type	Probe Height (m)	Damper Speed (steps/s)	Mean Wind Tunnel Speed (m/s)
Fig. 4.2	A100	Suburban	0.06	100,000	20
Fig. 4.3	A100	Suburban	0.06	100,000	20
Fig. 4.4	A100	Suburban	0.06	100,000	20
Fig. 4.5	A100 and B100	Open	0.06	100,000	15
Fig. 4.6	A150	All	0.1	150,000	15
Fig. 4.7	A30	Suburban	0.5	30,000	20
Fig. 4.8	A30	Suburban	0.5	30,000	20
Fig. 4.9	B100	Urban	0.1	100,000	15

4.2   Velocity

Figures 4.1 through 4.4 show the wavelet analysis for a laminar gust and all three velocity components of a turbulent gust. These figures all contain the velocity series analzed in the

upper plot with the wavelet coefficient map in the lower plot. Figure 4.1 also includes the turbulence intensity time series as the middle plot, and clearly shows that for low turbulence situations, the wavelets return very small coefficients. The lighter colors representing high wavelet coefficients near the edges are caused by end effects (19), and do not accurately represent the frequency content of the data at the times near the ends of the velocity vector. As the coefficient magnitude represents the power contained in the signal at a given time and frequency, it makes sense that for a low turbulence time series there would be low coefficient magnitudes, as is indeed seen in Figure 4.1. Following this logic, the brighter areas in Figures 4.2 through 4.4 should correspond in time to parts of the velocity where large changes in velocity are observed. Indeed, this was the case. Thus, the coloration was considered related to the turbulence intensity.

The approach to the data analysis, therefore, was to plot the wavelet coefficients for several gusts, and identify any similar structures, based on the coloration. If a gust had an effect on the boundary layer, a pattern of similar coloration would appear between gust cases. Both brightly and darkly colored events were sought. While it seemed most reasonable that similar patterns would appear around the time of the gust event (at 2500 samples on Figures 4.2 through 4.9), a similar structure occurring after the event was also sought. Figures 4.5 through 4.7 display a sampling of the wavelet coefficients for various gusts. While all the gusts do contain high energy and low energy structures, these structures not only occur with no correlation to the gust event, but also with no commonality between gust cases. As it would not be surprising to see this lack of commonality between gust cases with different parameters, as in Figure 4.5 which compares the two gust types, and in Figure 4.6 which compares gusts across terrains, several data runs using identical gust parameters were also compared. Figure 4.7 compares three test runs, randomly selected from the ten test runs performed, and clearly displays the absence of a consistent gust effect on turbulence intensity within the boundary layer.
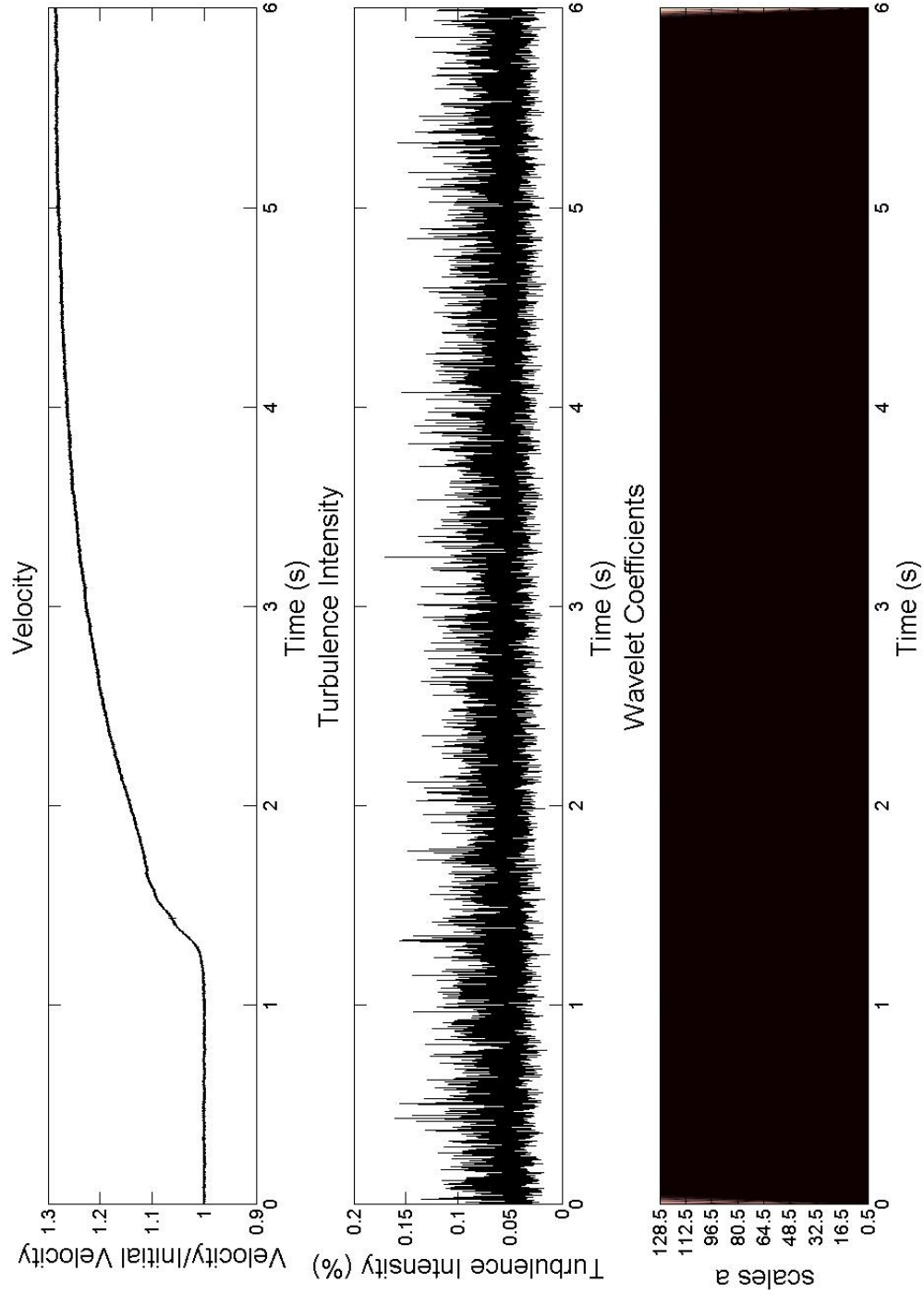
Figure 4.1 Velocity, turbulence intensity, and wavelet transforms for smooth gust A30 with free stream velocity of 15 m/s
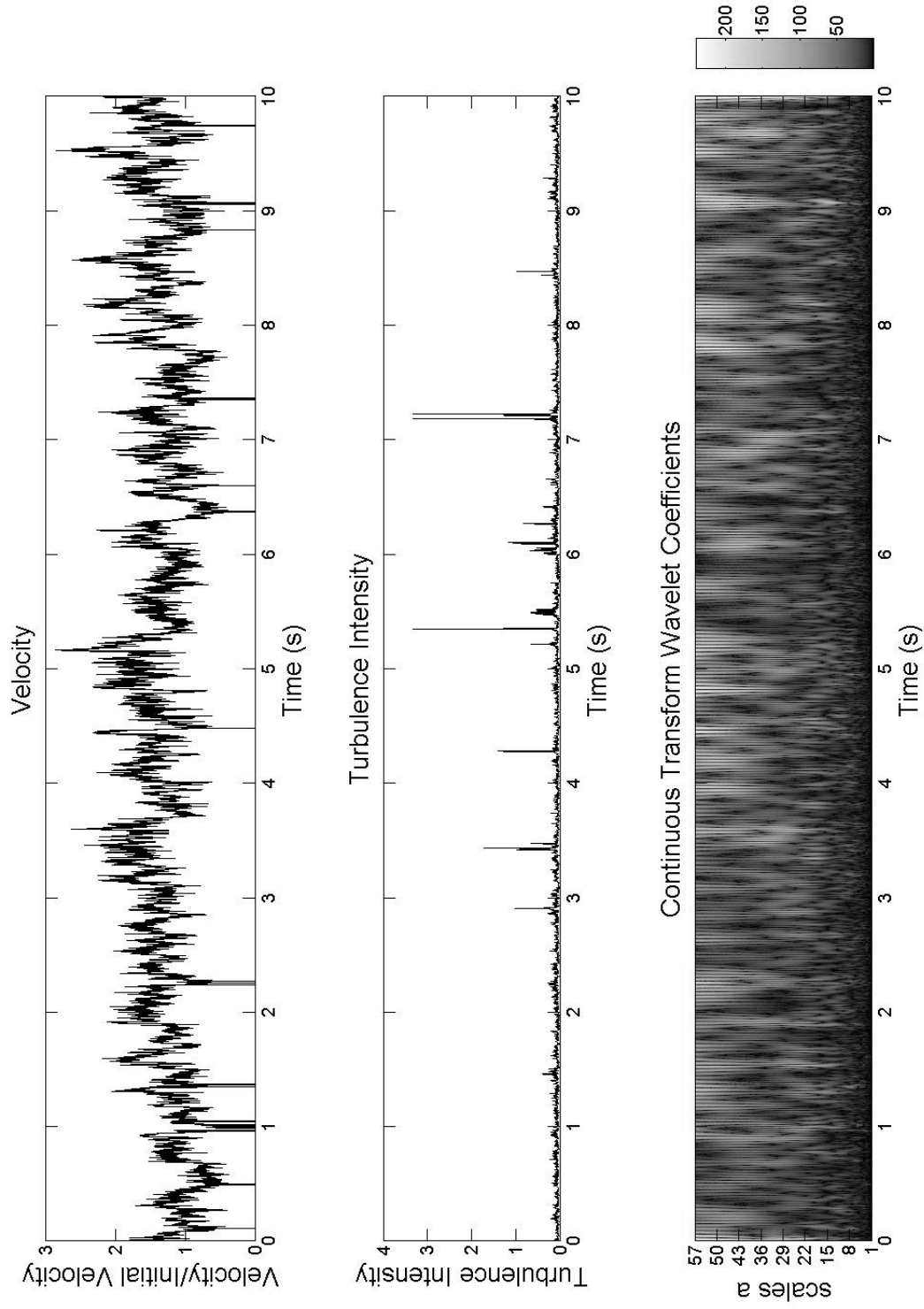
Figure 4.2 Suburban **U**, turbulence intensity, and wavelet transforms for Gust A100 with free stream velocity of 15 m/s at 6cm
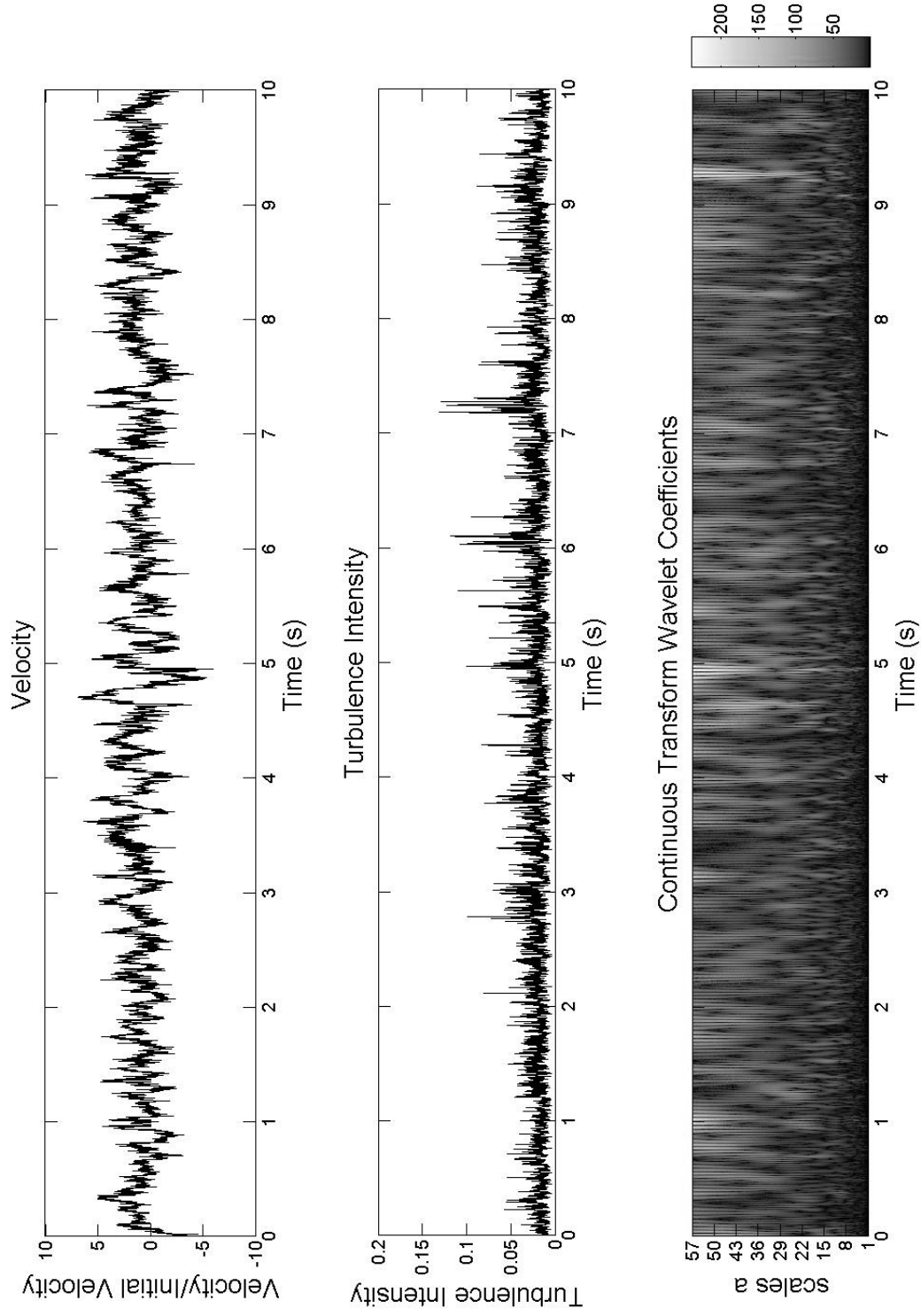
Figure 4.3   Suburban **V**, turbulence intensity, and wavelet transforms for
Gust A100 with free stream velocity of 15 m/s at 6cm
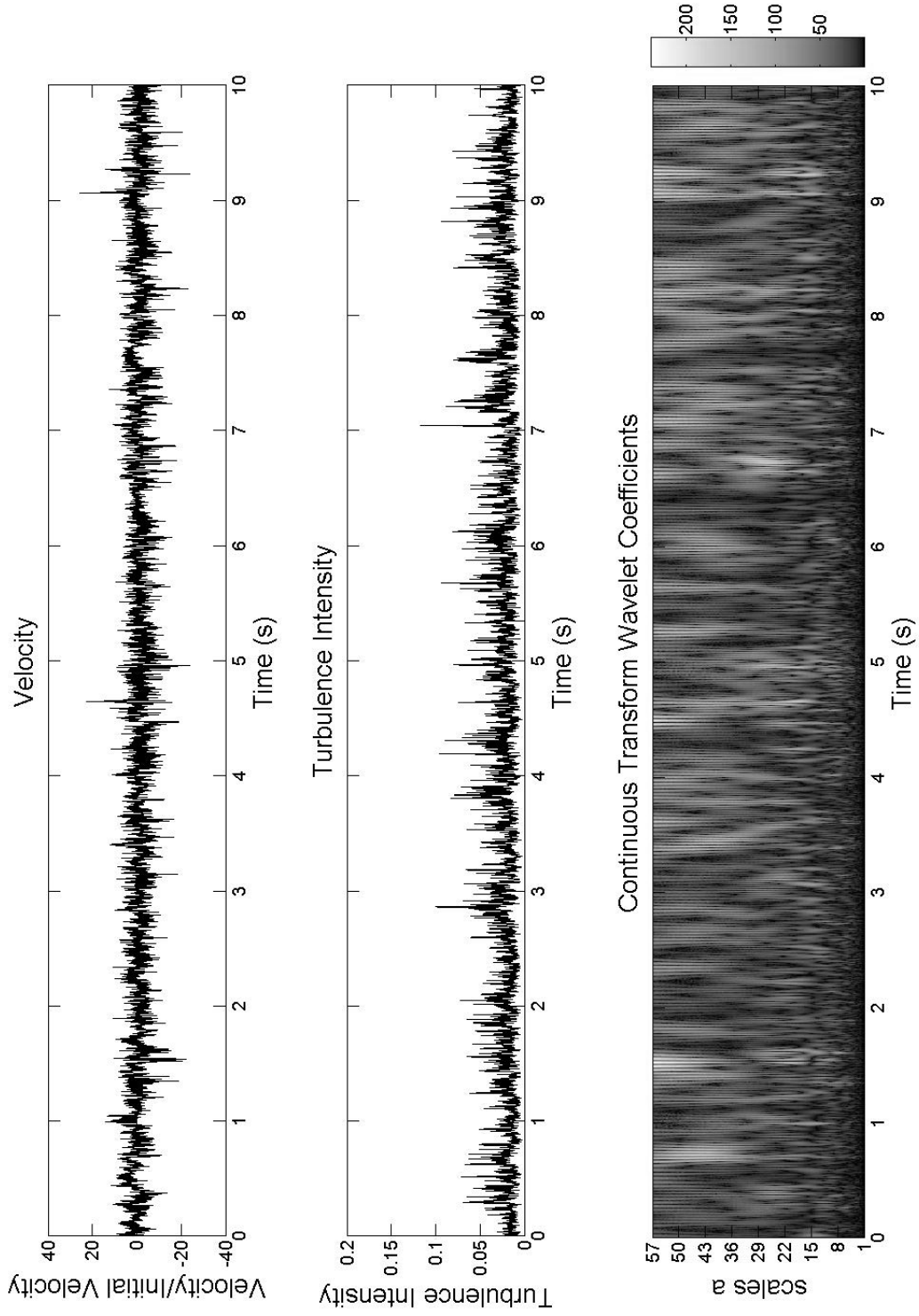
Figure 4.4 Suburban **W**, turbulence intensity, and wavelet transforms for Gust A100 with free stream velocity of 15 m/s at 6cm
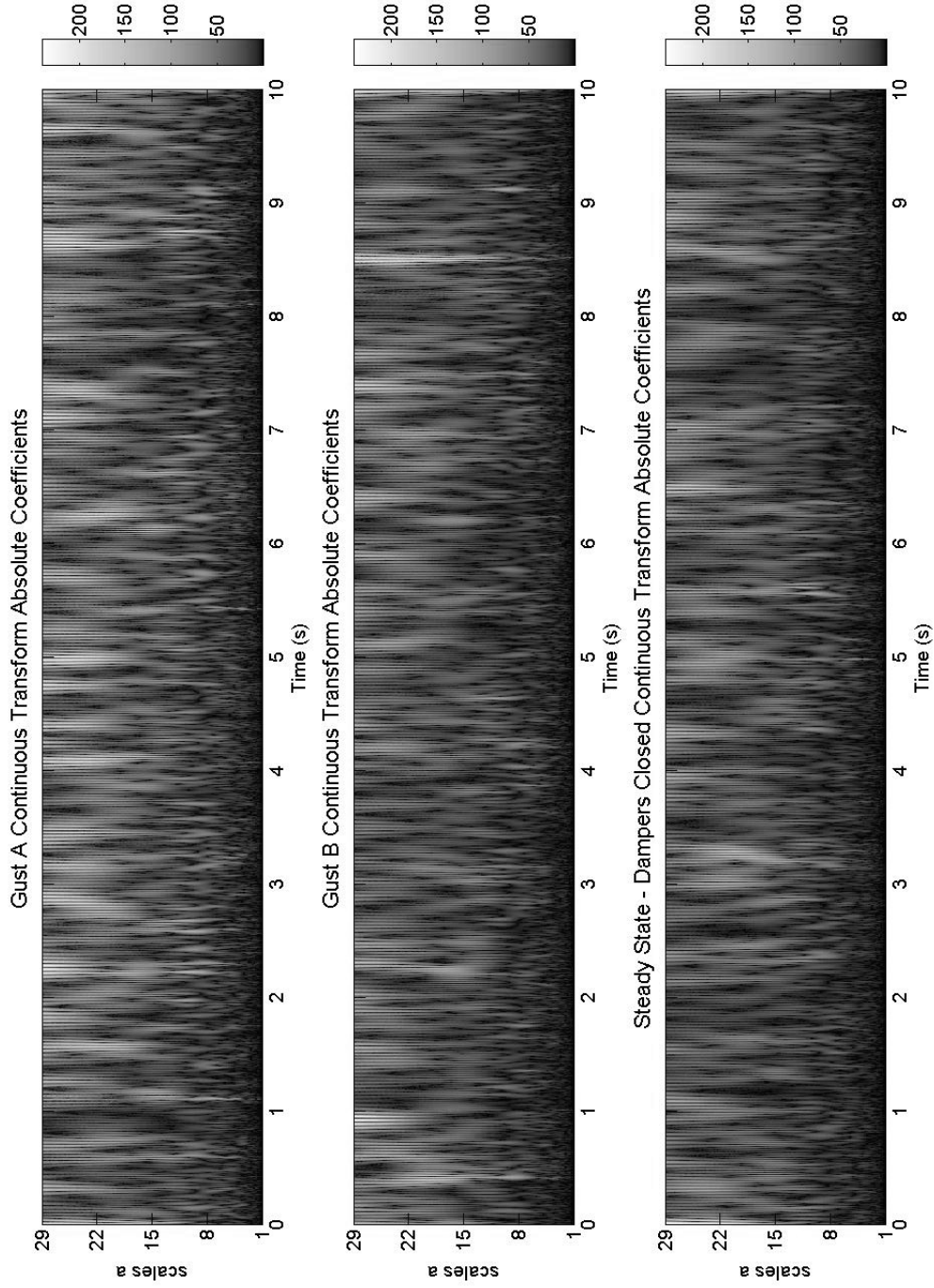
Figure 4.5 Comparison of open terrain Gust A100 and Gust B100 wavelet transforms with steady state flow with free stream velocity of 15 m/s at 6cm
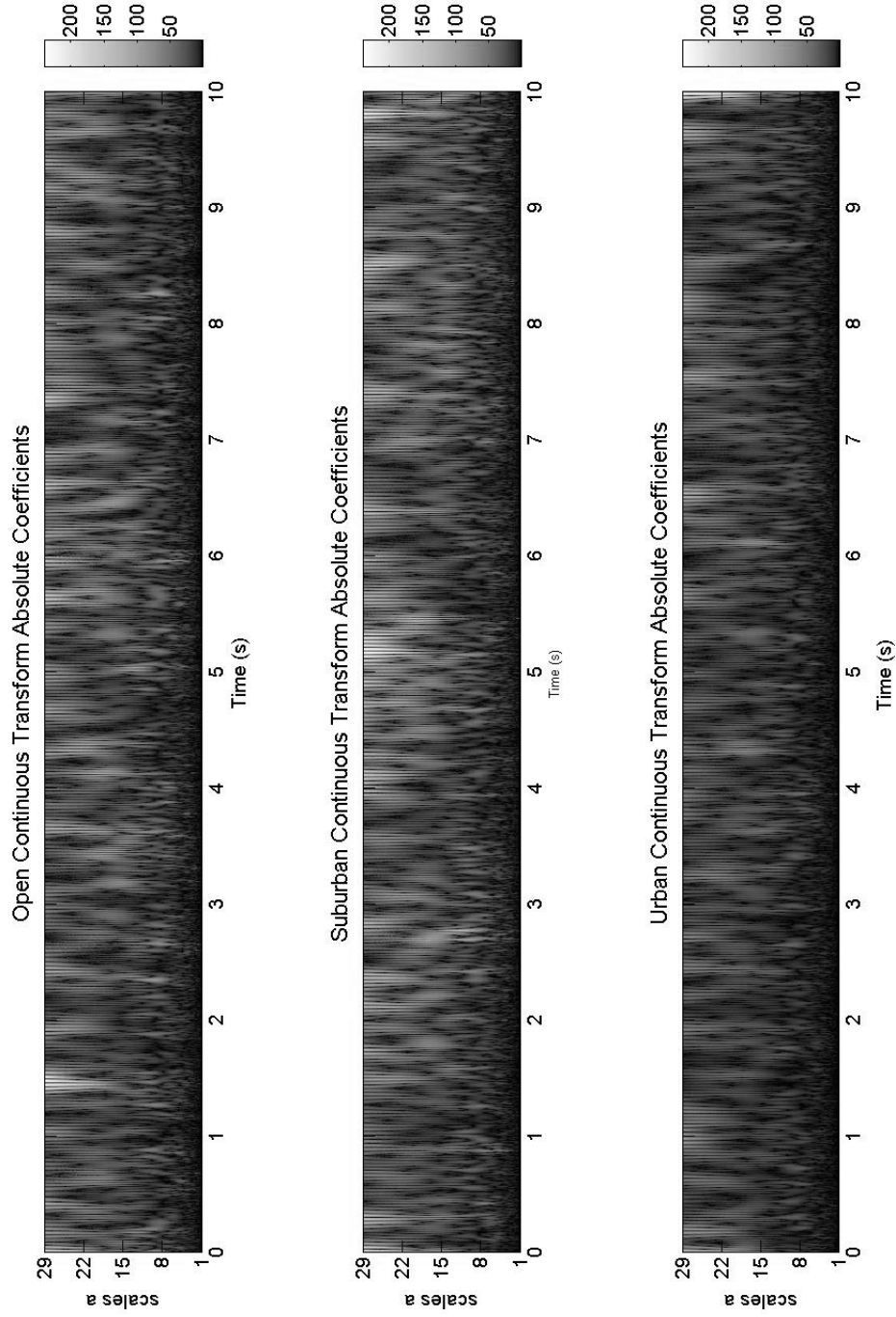
Figure 4.6 Comparison of all terrain wavelet transforms with steady state flow for Gust A150 with free stream velocity of 15 m/s at 10cm
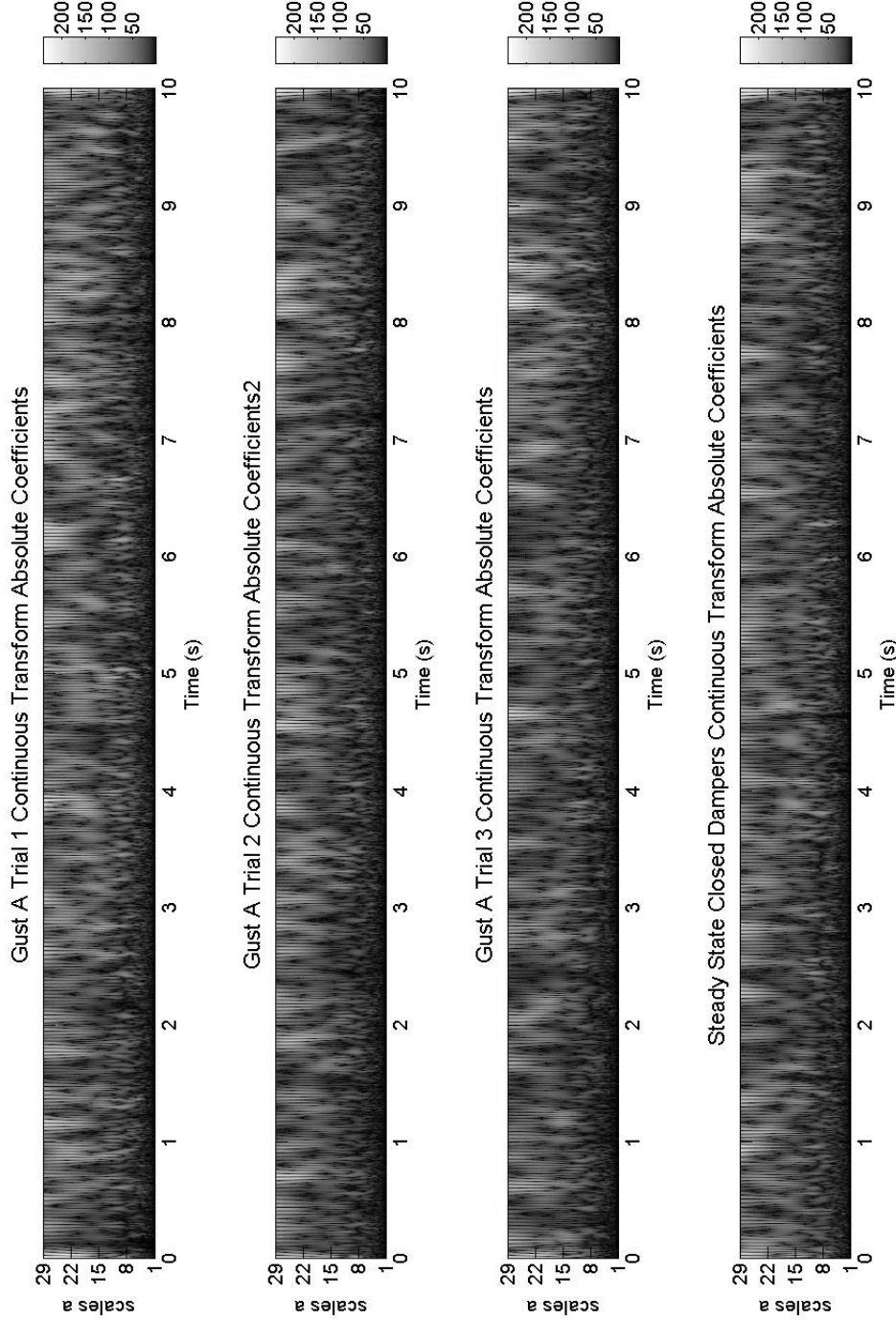
Figure 4.7 Comparison of three suburban gust trial wavelet transforms with steady state flow for Gust A30 with free stream velocity of 20 m/s at 50cm

4.3   Reynolds Stress

Hangan (21) used wavelet analysis of uv to find coherent structures in the wake of a cylinder. After discovering that the velocity profiles showed no effect of the gust upon the ABL, uv was investigated as another potential avenue to discover any effect of the gust event on the ABL structure. The turbulent components, u and v, were found using a variation of the time-varying turbulence intensity code. An average was taken over eleven points, then the value for u was computed as the difference between the center point value and the mean, as in Equations 4.1 though 4.3. The v and w components were calculated identically to the u component described in equations below.

Mean Velocity

$$meanU_i = \frac{1}{20} \sum_{j=i-5}^{i+5} U_i \tag{4.1}$$

Turbulent Velocity Component

$$u_i = U_i - meanU_i \tag{4.2}$$

Reynolds Stress

$$uv_i = u_i v_i \tag{4.3}$$

This system was run over the entirety of the velocity vectors in order to calculate the u, v, and w time series. The method used by Hangan (21) was used to look for high energy structures between the turbulent components. Additionally, the Reynolds stresses were calculated and analyzed with wavelets. Figure 4.8 shows that for one gust case, three trial runs had completely different high energy spots, indicating a lack of impact of the gust on the ABL in uv. Figure 4.9 contains all three Reynolds stresses, from a single data run, which also show no evidence of correlation to the gust event.

63

Figure 4.8 Comparison of three suburban uv trial wavelet transforms with steady state flow for Gust A30 with free stream velocity of 20 m/s at 50cm

Figure 4.9 Urban Reynold's stress wavelet transforms for Gust B100 with free stream velocity of 15 m/s at 10cm

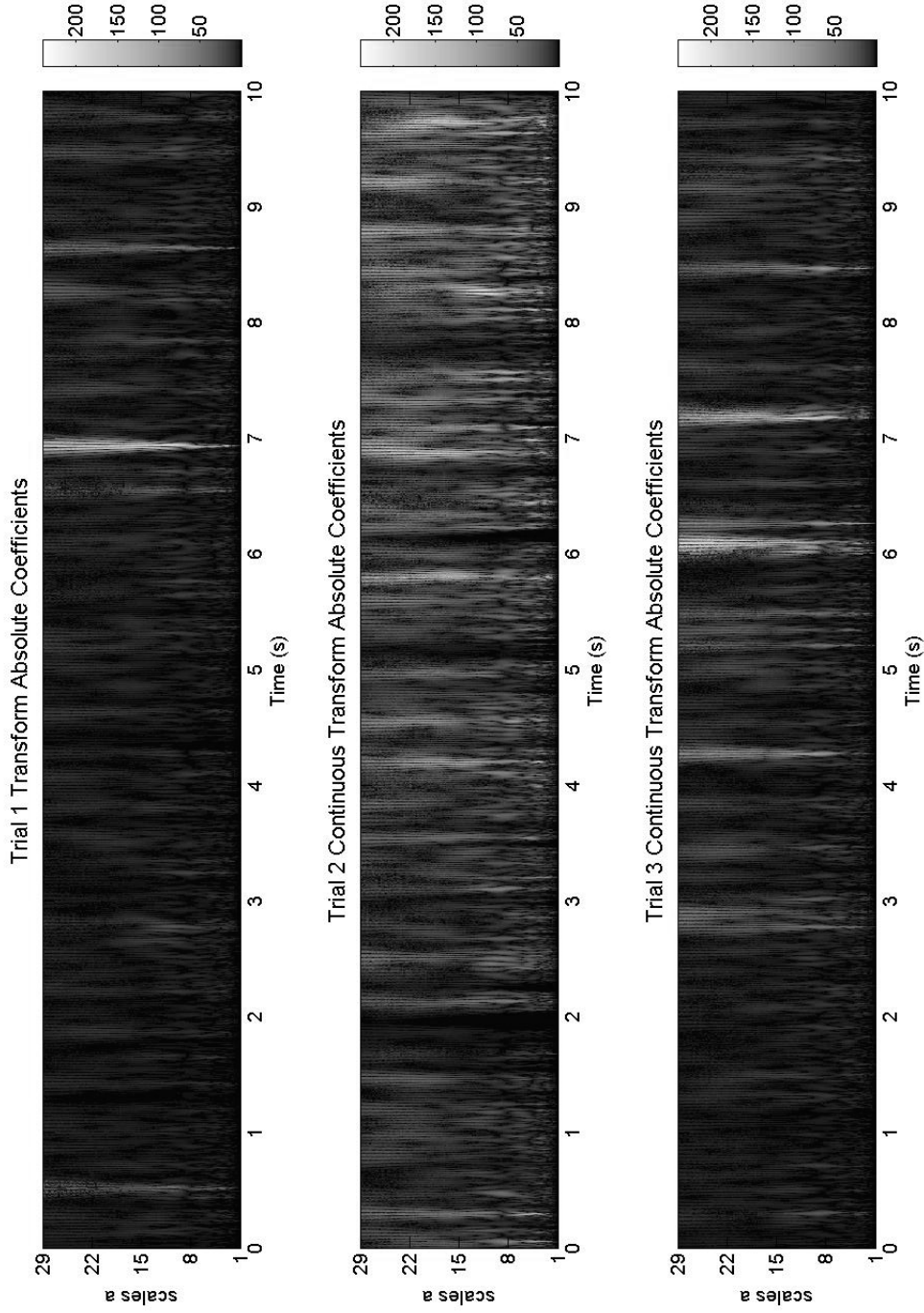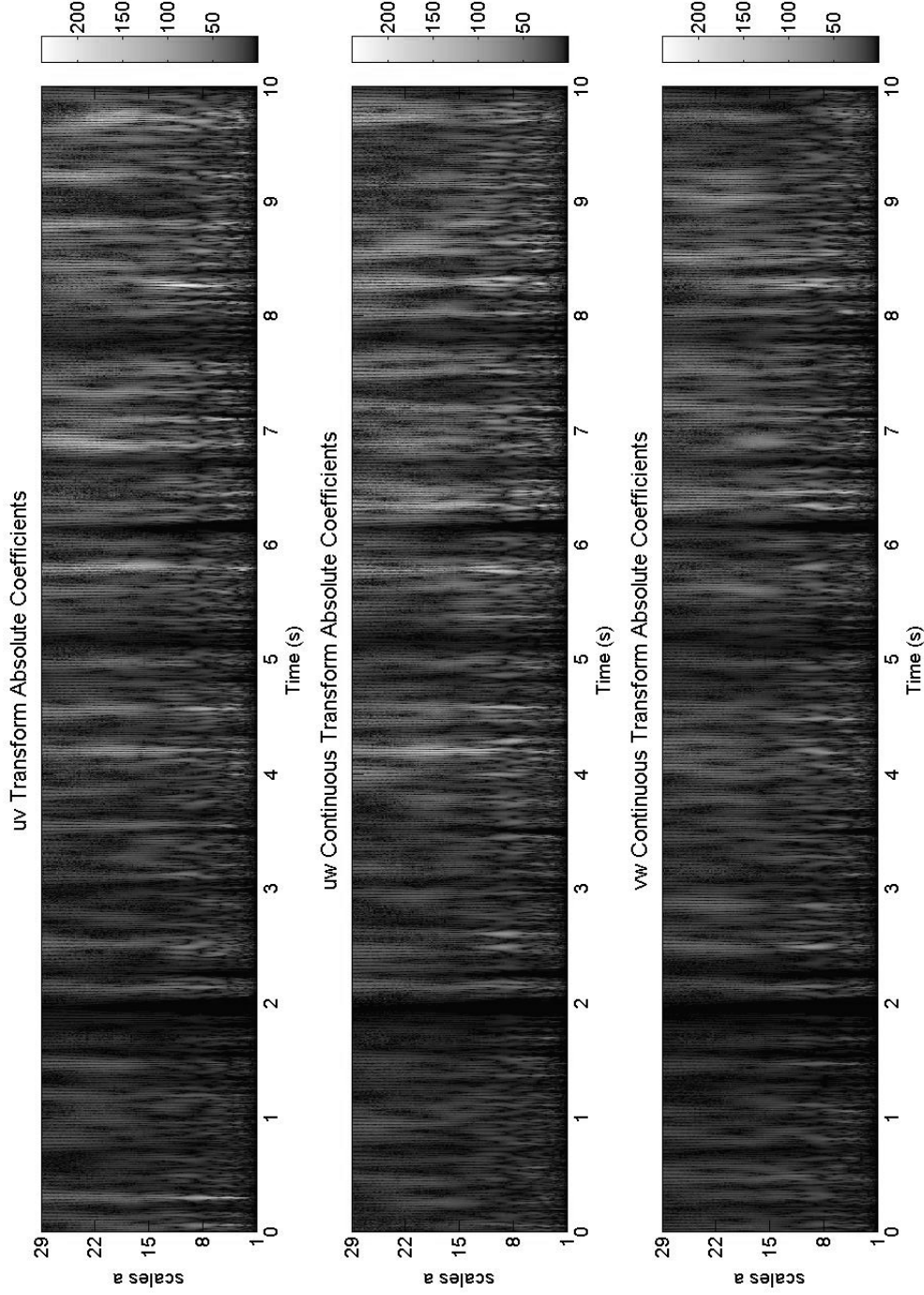# CHAPTER 5.   SUMMARY AND DISCUSSION

5.1   Summary of results

Atmospheric boundary layers at a 1:100 scale were successfully developed for open, suburban, and urban terrain in the AABL Wind and Gust Tunnel. During this development, various turbulence generators were studied. Triangular spires had the most influence upon the shape of the mean velocity profile and the turbulence intensity far from the floor. Floor roughness elements generated turbulence from the floor to 0.6 meters, while adding a wall significantly increased turbulence intensity throughout the entire boundary layer.

The capabilities of the AABL tunnel gusting system were explored, leading to enhanced understanding of the effects of the various parameters available. In general, the most dramatic gusts were generated with faster mean wind tunnel and damper closing speeds and greater closing distances. Using wavelet analysis, it was determined that the two types of gust explored had no obvious effect on the atmospheric boundary layer for any of the terrains developed.

5.2   Future work

For ABL generation, future work includes the design and testing of turbulence generators as additional boundary layers are needed. While most components can be developed based upon the trends discovered, more investigation of blocks may be required, as only one set of blocks was tested. It could be beneficial to conduct a series of experiments following Gartshore's methodology (13; 14) in order to develop empirical relationships between block geometry and ABL parameters for the AABL facility. While it was determined that the gust events explored had no noticeable effect on the ABL structure, there are other gust events and flow quantities to be explored. For example, opening and closing the gusting shutters periodically and larger

gusts generated with faster mean wind tunnel velocities could both produce a change in ABL structure. Reinforcing the wind tunnel near the fan is recommended before this is attempted, however. Another concept worthy of investigation is the possibility that the gust events are creating transient vortical structures. This investigation would require a vertical array of hot wire probes or a high speed particle image velocimetry system that would capture transent horizontal velocity.

APPENDIX A.   MATLAB CODES

Initial Processing

This code reads in data files, separates out the vectors, and saves and plots the data in various ways.

```
 %This program was written to work with Emi's Cobra probe time series
%output files.  They must be converted to ASCII form before this
%program will run them, and the header info must be deleted.
clear all


Data = load ('filename')
% Data2 = load ('-ascii', 'filename');


% Data = load ('filename')


U(:,1) = Data(:,1);
V(:,1) = Data(:,2);
W(:,1) = Data(:,3);
Pstatic(:,1) = Data(:,4);


 %For the hotwire laminar data
vel = Data(:,1);
vel = 0.0106*vel.^4 - 0.1248*vel.^3 + 0.9061*vel.^2 - 4.4028*vel + 8.42;
```

```
vel2 = Data2(:,1);
 vel2 = 0.0106*vel2.^4 - 0.1248*vel2.^3 + 0.9061*vel2.^2 - 4.4028*vel2 + 8.42;
 vel = decimate(vel,10);
vel2 = decimate(vel2,10);
 t = [1:103200]/8600;
t = decimate(t,10);
 figure
 hold on
plot(t,vel,'k')
 plot(t,vel2,'r')
legend('Gust A','Gust B')
xlabel('Time (s)')
 ylabel('Velocity (m/s)')


%Save the data as a set of matlab files in order to look at each component
%with the wavelet GUI


save ('filename')
save ('filename')
save ('filename')



%Find the mean initial velocity.
 Umean = mean(U(1:2500));
Uaftergustmean = mean(U(5000:37632));
Vmean = mean(U(1:2500));
Vaftergustmean = mean(V(5000:37632));
Wmean = mean(U(1:2500));
```

```
Waftergustmean = mean(W(5000:37632));


%Find the mean for the steady state cases

Umean = mean(U);

Vmean = mean(V);

Wmean = mean(W);


%For the laminar data
 velmean = mean(vel(1:8000));
%Normalize the time series by the mean initial velocity and plot

Unormal = U/Umean;

Vnormal = V/Vmean;

 Wnormal = W/Wmean;

 %laminar data

velnormal = vel/velmean;
```

Turbulence Intensity Time Series

This code calculates the time varying turbulence intensity and uv. It saves these vectors for use in the wavelet code.

```
  clear all


Data50 = load ('filename');

Data10 = load ('filename');

Data6 = load ('filename');


%For full 15 second series m = 37500
```

```
m = 30000;

n = (m/2500)*8600;


U50(:,1) = Data50(1:m,1);

V50(:,1) = Data50(1:m,2);

W50(:,1) = Data50(1:m,3);


U10(:,1) = Data10(1:m,1);

V10(:,1) = Data10(1:m,2);

W10(:,1) = Data10(1:m,3);


U6(:,1) = Data6(1:m,1);

V6(:,1) = Data6(1:m,2);

W6(:,1) = Data6(1:m,3);


lam = vel(1:n);


V50 = V50+30;

V10 = V10+30;

V6 = V6+30;

W50 = W50+30;

W10 = W10+30;

W6 = W6+30;



for i = 6:m-5

    Umean50(i-5) = mean(U50(i-5:i+5));

    Ustd50(i-5) = std(U50(i-5:i+5));
```

```
uprime50(i-5) = U50(i-5)-Umean50(i-5);

Umean10(i-5) = mean(U10(i-5:i+5));

Ustd10(i-5) = std(U10(i-5:i+5));

uprime10(i-5) = U10(i-5)-Umean10(i-5);

Umean6(i-5) = mean(U6(i-5:i+5));

Ustd6(i-5) = std(U6(i-5:i+5));

uprime6(i-5) = U6(i-5)-Umean6(i-5);


Vmean50(i-5) = mean(V50(i-5:i+5));

Vstd50(i-5) = std(V50(i-5:i+5));

vprime50(i-5) = V50(i-5)-Vmean50(i-5);

Vmean10(i-5) = mean(V10(i-5:i+5));

Vstd10(i-5) = std(V10(i-5:i+5));

vprime10(i-5) = V10(i-5)-Vmean10(i-5);

Vmean6(i-5) = mean(V6(i-5:i+5));

Vstd6(i-5) = std(V6(i-5:i+5));

vprime6(i-5) = V6(i-5)-Vmean6(i-5);


Wmean50(i-5) = mean(W50(i-5:i+5));

Wstd50(i-5) = std(W50(i-5:i+5));

wprime50(i-5) = W50(i-5)-Wmean50(i-5);

Wmean10(i-5) = mean(W10(i-5:i+5));

Wstd10(i-5) = std(W10(i-5:i+5));

wprime10(i-5) = W10(i-5)-Wmean10(i-5);

Wmean6(i-5) = mean(W6(i-5:i+5));

Wstd6(i-5) = std(W6(i-5:i+5));

wprime6(i-5) = W6(i-5)-Wmean6(i-5);
```

```
    t(i-5) = (i-5)/2500;


end


uv10 = uprime10.*vprime10;

uw10 = uprime10.*wprime10;

vw10 = wprime10.*vprime10;


uv50 = uprime50.*vprime50;

uw50 = uprime50.*wprime50;

vw50 = wprime50.*vprime50;


uv6 = uprime6.*vprime6;

uw6 = uprime6.*wprime6;

vw6 = wprime6.*vprime6;


save('filename');
save('filename');
save('filename');
```

Wavelets

This code analyses the data from either of the above codes using the continuous Morlet wavelet. It can display the wavelet coefficients in various ways.

```
clear all
```

```
m = 10000;

n = (m/2500)*8600;


load ('filename')

load ('filename')

load ('filename')

u = U(1:m);

v = V(1:m);

w = W(1:m);

load ('filename')

load ('filename')

load ('filename')

u3 = U(1:m);

v3 = V(1:m);

w3 = W(1:m);

load ('U.mat');

load ('V.mat');

load ('W.mat');

u5 = U(1:m);

v5 = V(1:m);

w5 = W(1:m);


%Load stress data

load ('filename')

uv = uv10(1:m);

load ('filename')

uw = uw10(1:m);

load ('filename')
```

```
vw = vw10(1:m);


%Load laminar data
load ('vel.mat');
vel = vel(1:m);


%Use this to plot several scalograms in one figure
figure
subplot(311)
ucoefs = cwt(uv,1:128,'morl','glbabs');
title('uv Test 1 Continuous Transform Absolute Coefficients')
subplot(312)
ucoefs3 = cwt(uv2,1:128,'morl','glbabs');
title('uv Test 2 Continuous Transform Absolute Coefficients')
subplot(313)
ucoefs5 = cwt(uv3,1:128,'morl','glbabs');
title('uv Test 3 Continuous Transform Absolute Coefficients')



figure
vcoefs = cwt(v,1:128,'morl','3Dglbabs');
title('Open Continuous Transform Absolute Coefficients')
figure
wcoefs = cwt(w,1:128,'morl','glbabs');


figure
velcoefs = cwt(vel,1:128,'morl','glbabs');
uvcoefs = ucoefs.*vcoefs;
```

```
vwcoefs = vcoefs.*wcoefs;

uwcoefs = ucoefs.*wcoefs;

uvelcoefs = ucoefs.*velcoefs;


%wavelet coherence function

uvco = (abs(uvcoefs.*uvcoefs)./(ucoefs.*vcoefs)).^0.5;

uvco = real(uvco);

figure

image(uvelcoefs)

colormap(pink)

title('Correlation between Cobra U and Laminar Vel')

figure

image(uvco)

colormap(jet)

title('UV Coherence')
```

APPENDIX B.   ADDITIONAL DATA

Supplemental Statistics

More stuff.

BIBLIOGRAPHY

[1] F.L. Haan, Jr., P.P. Sarkar, N. Spencer-Berger, Development of an active gust generation mechanism on a wind tunnel for wind engineering and industrial aerodynamics applications. *Wind and Structures,* 9(2006).

[2] American Society of Civil Engineers (ASCE). "Minimum design loads for buildings and other structures." *ASCE 7-05*, ASCE, 2005.

[3] Architectural Institute of Japan (AIJ). "Recommendations for loads on buildings." AIJ. (1996).

[4] Stull, Roland B. *An introduction to boundary layer meteorology* Dordrecht: Kluwer, 1988.

[5] Fang, C., B.L. Sill. "Aerodynamic roughness length: correlation with roughness elements." *Journal of Wind Engineering and Industrial Aerodynamics* 41-44(1992): 449-460.

[6] Tieleman, Henry W.. "Wind tunnel simulation of wind loading on low-rise structures: a review." *Journal of Wind Engineering and Industrial Aerodynamics* 91(2003): 1627-1649.

[7] De Bortoli, M.E., B. Natalini, M.J. Paluch, M.B. Natalini. "Part-depth wind tunnel simulations of the atmospheric boundary layer." *Journal of Wind Engineering and Industrial Aerodynamics* 90(2002): 281-291.

[8] Ho, T.C.E., D. Surry, D. Morrish, G.A. Kopp. "The UWO contribution to the NIST aerodynamic database for wind loads on low buildings: Part 1. Archiving format and basic aerodynamic data." *Journal of Wind Engineering and Industrial Aerodynamics* 93(2005): 1-30.

[9] Farell, Cesar, Arun K.S. Iyengar. "Experiments on the wind tunnel simulation of atmospheric boundary layers." *Journal of Wind Engineering and Industrial Aerodynamics* 79(1999): 11-35.

[10] Bienkiewica, B., M. Endo, J.A. Main, W.P. Fritz. "Comparative inter-laboratory study of wind loading on low industrial buildings." *ICWE12* (2007).

[11] Counihan, J. "An improved method of simulating an atmospheric boundary layer in a wind tunnel." *Atmospheric Environment* 3(1969): 197-214.

[12] Irwin, H.P.A.H., "The Design of Spires for Wind Simulation." *Journal of Wind Engineering and Industrial Aerodynamics* (1981): 361-365.

[13] Gartshore, I.S., K.A. De Croos. "Roughness element geometry Required for wind tunnel simulations of the atmospheric wind." *Journal of Fluids Engineering* (1977): 480-485.

[14] Gartshore, I.S., "A relationship between roughness geometry and velocity profile shape for turbulent boundary layers," N.A.E., LTR-LA-140, 1973, National Research Council of Canada.

[15] Tieleman, H.W. "Universality of velocity spectra." *Journal of Wind Engineering and Industrial Aerodynamics* 56(1995): 55-69.

[16] Burrus, C. Sidney, Ramesh A. Gopinath, Haitao Gao. *Introduction to Wavelets and Wavelet Transforms.* Upper Saddle River, NJ: Prentice Hall, 1998.

[17] Gurley, K., T. Kijewski, A. Kareem. "First- and higher-order correlation detection using wavelet transforms." *Journal of Engineering Mechanics* Feb.(2003): 188-201.

[18] Torrence, Christopher, Gilbert P. Compo. "A Practical Guide to Wavelet Analysis." *Bulletin of the American Meteorological Society* 79(1998): 61-78.

[19] Kijewski, T., A. Kareem. "On the presence of end effects and their melioration in wavelet-based analysis." *Journal of Sound and Vibration* 256(2002): 980-988.

[20] Kareem, A., T. Kijewski. "Time-frequency analysis of wind effects on structures." *Journal of Wind Engineering and Industrial Aerodynamics* 90(2002): 1435-1452.

[21] Hangan, H., G. A. Kopp, A. Vernet, R. Martinuzzi. "A wavelet pattern recognition technique for identifying flow structures in cylinder generated wakes." *Journal of Wind Engineering and Industrial Aerodynamics* 89(2001): 1001-1015.